THESIS

EFFECTS OF LABORATORY ELEVATION ON ROLLING THIN FILM OVEN TEST RESULTS

Submitted by

Haohang Wang

Department of Construction Management

In partial fulfillment of the requirements

For the Degree of Master of Science

Colorado State University

Fort Collins, Colorado

Summer 2013

Master's Committee:

Advisor: Scott Shuler

Suren Chen
Rodolfo Valdes-Vasquez.

ABSTRACT

EFFECTS OF LABORATORY ELEVATION ON ROLLING THIN FILM OVEN TEST

Asphalt is the most commonly used material for road pavement. Asphalt pavement provides low cost, high durability, superior waterproofing abilities, and rapid construction. Before laying down the actual pavement, a series of tests are performed to make sure the asphalt can meet the requirements on specifications. The tests are usually conducted twice. One is provided by the asphalt supplier, the other one is provided by the buyer to make sure the quality of the asphalt meets their requirements. The asphalt aging process is unavoidable and starts when the asphalt is produced. The Rolling Thins Film Oven test (RTFO) is used to simulate the aging from production to asphalt laydown. The Dynamic Shear Rheometer (DSR) is used to quantify asphalt's elastic and viscous properties, which can reflect asphalt's ability to resist deformation during its service life. The goal of this paper is to identify any trends with respect to elevation, including which binders are influenced by elevation change. The general hypothesis is that elevation can affect both test results from DSR and Ductility tests. If this is true, then the test results from specs might need to be adjusted when bringing asphalt from one elevation to another. E.g. If the supplier is at sea level and the buyer is at 6000 feet, the supplier's test results may perfectly match the specs at sea level, but when the asphalt is tested in the same way at 6000 feet, the result cannot meet the requirements. This means the supplier is at the risk of not getting paid. In this case, the specs need to be adjusted for a situation like this.

By analyzing the test parameters from DSR and ductility test, my research showed

that the elevation can affect the test results. The DSR test parameters are G*, δ, G*/sin δ, G*-6C, δ-6C, and G*/sin δ -6C.

Complex modulus (G*) reflects the specimen's total resistance to deformation when repeatedly sheared. The bigger the G* value, the stiffer the asphalt binder is. Phase angle (δ) indicates the lag between the applied shear stress and the resulting shear strain. G*/sin δ is the rutting parameter. When DSR was conducted at -6C, it can achieve G*-6C, δ-6C, G*/sin δ -6C. The seven different performance grades of asphalt specimens were PG 64-22, PG 64-28, PG 64-34, PG 70-22, PG 70-28, PG 76-22 and PG 76-28. Results showed that test parameters of certain asphalt performance grades present linear regression as elevation goes up. E.g. G* value decreases as elevation goes up, in the corresponding asphalt binders PG 64-22, PG 64-34, PG 70-28, and PG 76-22. Parameter G*, δ, G*/sin δ, G* -6C, δ -6C, G*/sin δ -6C shows clear linear regression as elevation goes up. Ductility did not present obvious linear regression as elevation goes up, therefore, is omitted from the summary. The discrepancy may have resulted from insufficient test data. The recommendation is that the researchers continue collecting data on ductility properties test. When using PG 70-28 for DSR test, test parameters presented linear regression as elevation goes up. The test parameters are G*, δ, G*-6, δ- 6C. When using PG 76-22 in the DSR test, test parameters presented linear regression as elevation goes up. The affected test parameters are G*, δ, G*/sin δ, G*-6C, and G*/sin δ -6C. Logically, if δ is affected by elevation, then δ-6C should also be affected by elevation. Thus, the assumption that δ-6C does not present linear regression as elevation goes up was because of the insufficient data volume. If there had been three times more data pool than the data set in this paper, the assumption may be proved right.

ACKNOWLEDGEMENTS

It is with immense gratitude that I acknowledge the assistance of my committee chair, Professor Scott Shuler, who guided me to complete this paper. Without his advice and persistent help, this thesis would not have been possible.

I also would like to thank my committee members, Professor Suren Chen and Professor Rodolfo Valdes-Vasquez, for their time and support. I would also thank the Western Cooperative Test Group for providing data for this study.

TABLE OF CONTENTS

LIST OF TABLES

LIST OF FIGURES

LIST OF KEYWORDS

Asphalt

Oxidation

Pavement

Elevation

RTFO

INTRODUCTION

Asphalt General Background

Asphalt is a dark-brown to black cementitious material which is part of a family of materials known as bitumens that either occur in nature or are obtained in petroleum processing (*Standard, 2013*). Asphalt is mainly used in road construction by mixing with aggregate to make asphalt concrete. 94 percent of the roads in America are surfaced with asphalt (Asphalt Pavement Alliance, 2013). It is estimated that 500 million tons of Hot Mixed Asphalt (HMA) are placed annually at a cost of approximately $10.5 billion (Khsaibati & Stephen, 1999).

HMA is produced at temperatures of 275°F to 325°F. These elevated temperatures harden the asphalt binder. This hardening process can affect pavement performance and must be evaluated in the laboratory. The Rolling Thin Film Oven Test (RTFOT) is the procedure used to accomplish this (ASTM, 2013).

RTFO provides asphalt specimens for Dynamic Shear Rheomter (DSR) and Ductility test. RTFO simulates asphalt aging from production to lay down. DSR and Ductility are very important asphalt testing methods in quantifying asphalt's resistance to deformation. Complex shear modulus (G*), phase angle (δ) and rutting parameter (G*/sin δ) are test parameters from DSR test.

Problem Statement

The aim of this paper is to test the hypothesis that elevation can affect DSR and Ductility test results. If this assumption is true, it will present some problems with the current asphalt testing measuring standard. This is problematic because laboratories conducting the same test at one elevation may report different results from laboratories at another elevation. For instance, if the asphalt supplier is at sea level and the buyer is at 6000 feet, the supplier's test results on asphalt may perfectly match the specs, but when the asphalt is tested in the same way at 6000 feet, the result cannot meet the specs. This means the supplier is at the risk of not getting paid. In this case, the specs need to be adjusted for a situation like this. Yet, if the test results variance stays within the specs' tolerance on test results, then it is fine, we do not need to adjust the specs for this situation. If the test results variance is beyond the spec's tolerance, the specs should be adjusted to meet this situation. However, my current research is to find out if elevation can affect test results.

Research Questions

There are a couple of questions based on this research.

1. Do the test results present linear regression as the elevation goes up?
2. If the elevation does have an impact on test results, which tests parameters are affected by elevation?
3. If some parameters are affected by elevation, what performance grade asphalt is involved?

Relevant Tests

The research focuses on analyzing seven test parameters, G*, δ, G*/sin δ, G*-6C, δ-6C, G*/sin δ -6C and ductility. The relevant test parameters are detailed below:

Rolling Thin Film Oven Aging

The purpose of the RTFO is to simulate asphalt aging during manufacturing and construction of pavements. In RTFO test, the asphalt sample is periodically exposed to fresh air flow and heat during rolling. Since the asphalt cement in the RTFO test is continually moving fresh surfaces of the asphalt are exposed and aging is accelerated. The asphalt samples are placed in bottles, which are inserted in a rack in the oven at 325°F. The rack rotates at a specified rate around a horizontal axis. The rotating bottle continuously exposes fresh asphalt. Every time the sample bottle passes in front of an air vent during rotation, the vapors accumulated in the sample bottle are purged by the heated air from the jet (Robert, Kandhal, Brown, Lee & Kennedy, 1996).

Complex Shear Modulus, G*

The complex shear modulus evaluates the viscous and elastic behavior of asphalt binders at high and intermediate service temperatures. The dynamic shear rheometer is the apparatus utilized to measure G*. This test is operated by putting plate-shaped asphalt between a fixed plate and an oscillating plate. Strain is applied to the oscillating plate, and the time it takes for the torque to go one round is measured. Usually, the thickness of the binder sample sandwiched between the fixed plate and the spindle is determined by the test temperature. The higher the temperature, the thinner the sample required, and vice versa. DSR is used in the Superpave specification to measure the properties of the asphalt binder at high- and intermediate-pavement-service temperatures. The actual test temperatures are based on the anticipated in-service temperatures in which the asphalt binder will function. Complex shear modulus, G*, is the total resistance of the binder to deformation when repeatedly sheared. G* consists of two components, the storage modulus G’ (elastic, recoverable parts) and the loss modulus G” (viscous, non-recoverable parts). G’’ is a measure of the ability of an asphalt to relieve strain-induced stress by viscous flow and is the vector sum of G” and G’ as shown in Figure 1 (Goodrich, 1991).

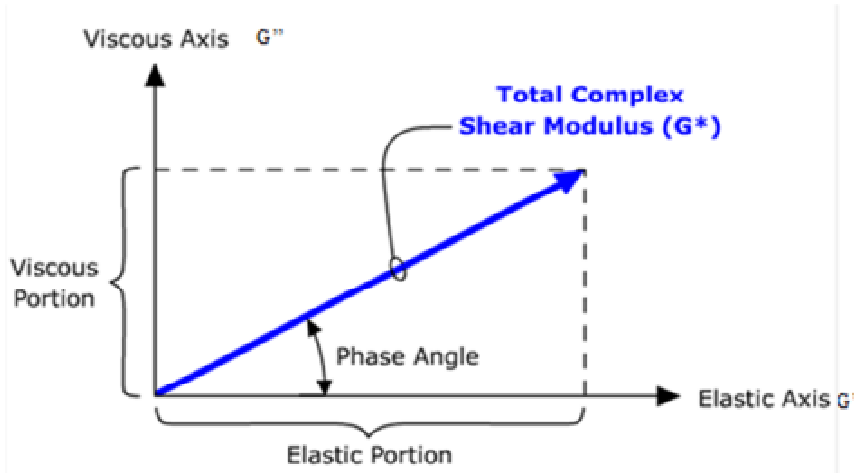

Figure 1: Complex Shear Modulus and Phase Angle Analysis

Temperature and loading frequency dramatically impact the value of G*. At low temperatures, asphalt tends to approach pure elastic behavior and becomes brittle, due to a lack of molecular motion which could thermally dissipate the applied strain energy.

Phase Angle, δ

The phase angle, δ, represents the relationship of the complex shear modulus to the elastic component of the complex modulus. Two asphalt binder samples can have the same G* but different phase angles when loaded. The asphalt with the larger phase angle tends to display more viscous or non-recoverable deformation and less elastic (recoverable) deformation (Pavement, 2008).

During the DSR test, the amplitude of the resultant stress is measured by determining the torque transmitted through the sample. The strain amplitude and frequency are input variables. The operator sets the parameter value. The phase angle is measured by determining the sin wave form of the input strain and the resultant torque response (Goodrich, 1991).

G*/sin δ

The ratio of complex shear modulus to the sin of δ after RTFO aging has been linked to permanent deformation performance of asphalt pavements (Stuart and Izzo, 1995). Consequently, this parameter is utilized in specifications to evaluate the quality of asphalt binders after aging.

Ductility

This test was considered as an important property of asphalt cement. The test is run in accordance with ASTM D113, it measures the distance in centimeters that a standard briquette of asphalt cement will stretch before breaking at a certain rate and temperature. It was believed by Roberts et al. 1996, that the low ductility is likely to show poorer service.

Research Approach

The data used in this paper is taken from round-robin testing organized by the Western Cooperative Test Group board members (WCTG). Based on the data provided by WCTG, SAS was used to analyze the data for all seven parameters to see if the test results present linear regression as elevation goes up and which PG asphalt contributes to that result. Plots are built to show the relationship between elevation and test results. The horizontal axis is the elevation, and the vertical axis is the test results. The test results are arranged in an order as elevation increases. The null hypothesis is considering the slope for parameters is zero. In looking at the T-test, if the P-value is smaller than 0.05, then the null hypothesis gets rejected. This means the test parameter presents linear regression as elevation goes up and the results are significantly different from others. A summary table of all the affected parameters and the relevant PG asphalt will be built and this can help the reader have a clear view of which parameters are affected and what kind of asphalt contributes to the result.

Key Results

The following parameters and binders were affected by elevation:

G*:	64-22, 64-34, 70-28 and 76-22
δ:	64-22, 64-34, 70-28 and 76-22
G*/sin δ:	64-22, 64-28, 64-34, 76-22 and 76-28.
G*-6C:	64-34, 70-28, 76-22 and 76-28
δ- 6C:	64-28, 70-28 and 76-28
G*/sin δ -6C:	64-28, 64-34, 76-22 and 76-28.

Recommendation and Implications

For the ductility test there is not enough data to analyze, *It sounds to colloquial.*so it is not discussed. As shown from the Key Results, among the affected test parameters G*, δ, G*-6C, and δ- 6C, PG 70-28 get affected by elevation. While PG 76-28 is influenced by elevation for parameter G*/sin δ, G*-6C, δ- 6C and G*/sin δ -6C. I assume PG 76-28 can also be influenced under parameter G* and δ. The reason why it does not prove my assumption was the lack of data. Thus, the recommendation is that the data providers can keep collecting data for these parameters. If a much bigger data pool for these parameters was achieved, the assumption can probably be proved right.

LITERATURE REVIEW

Since this research perspective is trying to find if DSR and Ductility test results can be affected by elevation, which is so unique, it is difficult to find similar research topic. The literatures reviewed in this chapter provide a general view of how the tests are analyzed by other researchers. It also shows the importance of the RTFO, DSR and ductility tests. This will assist the reader in better understanding the importance and background of the mentioned asphalt tests.

Mercado, Martin, Park, Spiegelman and Glover (2005) illustrated and analyzed the asphalt aging process from production to construction. The article noted that the U.S. Department of Transportation (DOT) maintains quality control (QC) and quality assurance (QA) programs that require asphalt binder testing to verify grade compliance according to Superpave performance grade (PG) specifications. Before the actual paving take place, asphalt may be transferred many times for storage or delivery, so binder properties may change, thereby creating a negative impact on binder performance. In order to find out which factors have a detrimental impact on asphalt's properties, a lab test was conducted to simulate the effects of storage time, storage temperature, contamination, and modification on the DSR after the RTFO-aging process. Their goal of this study was to help the Texas DOT identify factors with a critical damaging impact on binder properties prior to construction.

After the production process, asphalt is typically stored in the supplier's tank until it can be sent to a pavement site or HMA plant. The experience in Texas showed that the poor performance observed during the early life of a pavement may be related to significant changes in binder properties in the period between production and construction.

The authors used data extracted from Quality Control (QC) and Quality Assurance (QA) to track binder quality and provide guidance to improve the manufacturing process. They analyzed various factors that may affect the binder properties prior to construction including changing crude source, refinery process, blending, contamination with binders of different grades, length of storage time, and storage temperature. During the transfer line and transportation process, storage temperature and separation were considered as major factors. On the contractor's site, dilution, presence of modifier, contamination with binders of different grades, storage time, and storage temperature were regarded as main elements (Epps, Park, Arambula, and Spiegelman, 2002).

Initially, the authors intended to search for corresponding supplier and field sample test results and evaluate the changes. However, they realized that this method might not be successful due to the difficulties in collecting and matching supplier and field data. They then introduced a lab test to simulate four of the aging factors: storage time, storage temperature, contamination with binders of different grades, and the presence of a modifier. They used 1 week, 1 month and 2 months as three different storage time lengths. Three contamination statuses were identified: no contamination, contamination in the transfer line and transportation process, and contamination in the contractor's storage tank. Modifier levels included polymer-modified and unmodified. Two levels of suppliers were selected. A statistical discovery software, JMP, was used to define the combinations among the selected factors and their levels. The average value of two $G^*/\sin\delta$ readings on each sample is shown as the RTFO-DSR test result for each treated sample.

A Fourier Transform Infrared Spectroscopy (FTIR) test was performed on all samples.

FTIR is an analytic technique used to identify functional groups by measuring the absorption of various infrared light wavelengths by an irradiated sample (Jemison, Burr, Davison, Bullin, and Glover, 1992). FTIR is used to track oxidation related to binder aging in order to better understand and explain RTFO-DSR test results.

Test results were examined by using analysis of variance (ANOVA) to detect the statistically significant main effects and two-way interactions of the selected factors with a level of significance of 5%. The test results from FTIR spectral readings indicated that an oxidative process in the binder caused the relative change in the RTFO-DSR parameter $G^*/\sin\delta$.

The flaw of this test is that the selection of the storage time length was based on field experience; there were not enough scientific facts to support it. In addition, the authors did not explain how they measured the contamination levels or the potential contamination statues difference that could occur in each of the levels (e.g., the truck's insulation and its preheated tank's temperature might also impact the aging).

In another notable paper, Colbert, Beale, and You (2011) from Michigan Technological University used simulated aging techniques to analyze potential low temperature cracking of aged asphalts. Recycled Asphalt Pavement (RFP) and artificially-aged asphalt binders were characterized. RTFO and PAV were used to age binders, and the Asphalt Binder Cracking Device (ABCD) was used to investigate low temperature binder properties.

The authors believed the aging of pavement and pavement temperature affect asphalt binders' ability to withstand thermal cracking. The experimental plan involved extracting and recovering the RAP binder before testing for low temperature cracking, using RTFO and PAV to age virgin asphalt binders, and testing binders for low temperature performance using ABCD (Colbert et al., 2011). The virgin asphalt went through the RTFO for short-term aging and PAV multiple times for long-term aging simulation. ABCD used an environmental chamber which lowered the binder temperature according to user specifications. After heated asphalt was poured into four silicon molds, thermal cracking strain and temperature were recorded. (Zirlin et al, 2009). The testing specimens were a PG 58-28 control binder, 50% original binder/ 50% RAP binder blend, and a 100% RAP binder (Colbert et al, 2011).

Conclusions drawn from these tests indicated that the binder that underwent PAV aging had a higher thermal cracking temperature. The thermal cracking strain can be increased if the binder is PAV-aged. Tests results showed that an average 5.9% difference in thermal cracking temperature was observed when comparing the control binder versus artificially-aged binders, so the RTFO- and PAV-artificial-aging methods can simulate binder aging accurately.

In another intriguing study, Zhou, Li, and Zhang (2009) explored the high temperature performance of a binder containing fibers, since fibers had a history of use in civil engineering and could provide three-dimensional reinforcement for the mixture. They decided to investigate if asphalt mixed with fibers was any different than asphalt mixed with virgin binder under high temperature.

The Polypropylene fiber, polyester fiber, and cellulose fibers were used as modifiers. Asphalt material was graded as AH-70#; with a penetration of 67dmm at 25C, and a softening point of 61º C. DSR testing was used to identify the rheological properties of the binders at different temperatures. A Wheel Tracking device was used to evaluate the high-temperature resistance to rutting. The fiber-asphalt was prepared in a steel mold and a wheel load with pressure of 0.7±0.05MPa was applied. The traveling distance of the wheel was 230±10mm, the speed of the wheel was 42±1 rpm, the entire test took 60 minutes, and the temperature was 60±1ºC.

$$DS=\frac{S\times T}{D_{60}-D_{45}}$$

D60, the deflection at the elapsed loading time of 60 minutes, unit is mm.

D45, the deflection at the elapsed loading time of 45 minutes, unit is mm.

S is the wheel speed, which is 42 cycle/min.

T is the time difference, 15 minutes.

Rutting parameter (G*/ Sin δ) was used to evaluate the durability of asphalt mix. The higher G*/ Sin δ is at high temperature, the more durable the binder. The fiber-asphalt mix and asphalt with no fiber had a similar trend: rutting resistance went down as the temperature increased. However, the fiber-asphalt performed better than the sample without fiber. In a side-by-side comparison, polypropylene had the best performance, followed by polyester and cellulose. The control specimen had the lowest performance against rutting.

Zhou et al. (2009) concluded that the addition of fibers caused the asphalt-fiber mixture to demonstrate a permanent deformation resistance. Using the wheel tracking device, there is a peak value of DS with the increase of fiber content. This test sufficiently showed that fiber can increase the performance of asphalt. It also demonstrated the importance of the DSR test in binder performance analysis. However, because the aging situation was not discussed in the paper; there is a possibility that the fiber-asphalt has a different aging time or sensitivity to aging.

Similarly, research conducted by Al-Khateeb and Al-Akhras (2011) aimed to find the effect that cement additive can create on an asphalt binder’s properties. They wondered if Portland cement might be used as a filler or additive to improve the properties of asphalt binders and HMA mixtures. Polymer-modified asphalt binders can significantly improve resistance to rutting and thermal cracking, while also reducing fatigue damage, stripping, and temperature susceptibility. Hydrated cement can be used to produce emulsified asphalt, which can increase strength and durability of asphalt mixtures. In testing, black carbon was utilized as filler in the asphalt mixtures to enhance the viscosity, and sulfur was added to decrease the binder’s viscosity. When adding Portland cement and lime to asphalt binder, its resilient modulus, tensile strength, and resistance to moisture damage were strengthened.

The test binder was PG 64-10 which was supplied by Jordan Petroleum Refinery. There were 6 different cement-to-asphalt (C/A) ratios prepared. Each sample was prepared using a mechanical mixer at a temperature range of 145-152C. The temperature was determined based on the American Society for Testing and Materials (ASTM) temperature-viscosity relationship. A DSR test was conducted by applying shearing force to a thin asphalt disc sandwiched between two plates. The lower plate was fixed and the upper plate oscillated back and forth across the asphalt sample at a frequency of 10 rad/s. The complex shear modulus and phase angle were measured. G* values at different temperatures were plotted with the C/A ratio. The effect of the C/A ratio on the phase angle was also illustrated in a figure.

The results showed that the elastic behavior of the asphalt material remained the same with the addition of the Portland cement material. As the C/A ratio increased, the G* value also climbed. Results indicated that the C/A ratio can reflect the stiffness of asphalt binder. A C/A ratio of 0.15 was the optimal ratio to achieve a balanced increase in the value of DSR G*/Sin δ rutting parameter of binders.

The test method applied in the Al-Khateeb & Al-Akhras (2011) study provided a framework for analyzing the data that was achieved from WCTG, because it was thorough at illustrating the relationships among different samples and testing conditions.

Another important aspect of the literature was the relationship between asphalt compatibility, flow properties, and oxidative aging as presented by Pauli and Huang (1997). Embrittlement of asphalt pavement was impacted by changes in the flow properties of the binder. The colloidal-suspension model of asphalt was introduced to investigate asphalt composition changes after oxidation. Corbett separation (ASTM D4124-09) was used to categorize unaged and aged samples. The Christensen-Anderson-Marasteau (CAM) model was modified to create master curves for asphalt composition change in rheological properties after oxidation.

Gandhi, Akisetty, and Amirkhanian (2010) hypothesized that asphalt oxidation impacts the flow properties of the material in an embrittlement state. To predict differences in the rates of material embrittlement, oxidized asphalt samples' compositional and rheological properties were tested. The data in this paper was drawn from both literature and testing. Nine types of asphalts studied during the SHRP were selected for analysis. RTFO was used for the first-step aging and PAV for further aging. The oxidation process took three different time lengths, and each sample was analyzed for rheological properties by using an Ares rheometer.

Graphs from this paper showed the relationship between asphalt composition and viscoelasticity. Under a colloidal-suspension model, asphalt samples were sorted as either less compatible or more compatible in regards to their flow properties. Results showed that more compatible asphalts exhibited more ductility than less compatible asphalts. In terms of the relationship between flow properties and oxidation, the CAM model was applied to construct time-temperature master curves. The complex modulus increased as the aging time increased at a given frequency.

Rheological and compositional properties of un-aged and aged asphalt samples can be considered in order to generate aging master curves based on the CAM model. The parameter generated from these aging master curves is useful for measuring asphalt compatibility (Gandhi et al., 2010).

Ductility is another important property of evaporated residue of modified emulsion asphalt, as shown in research by Fu, Liu and Jing, 2009. The authors wondered if a modified asphalt binder treated by emulsion would exhibit a change in ductility, and so they investigated the influence of several different factors on the ductility of the evaporated residue of emulsified asphalt. The emulsifier, stabilizer, and the solution PH value were all analyzed.

Fu et al. (2009) used three different types of modified asphalt samples, A1, A2, and A3, with different ductility, penetration, and softening point values. The emulsifier and stabilizer were added to water to form an emulsion, and the mixture was heated up to approximately 78°C until it became transparent. The hot modified asphalt sample was poured into the emulsion, and a high-speed shearer was used to stir it until fully mixed. Then the modified emulsion asphalt was ready for testing and analyzing. There were two types of emulsifiers, E1 and E2. The figures showed that when E1 was added, ductility of the evaporated residue of modified emulsion asphalt A1 and A2 was reduced to different degrees. When E2 was added, the ductility of the evaporated residue of modified emulsion asphalt A2 and A3 decreased. This indicated that the ductility of different modified asphalts and emulsion mixture varies.

Both organic and inorganic stabilizers were used in these tests. Data showed that the ductility of evaporated residue increased as more stabilizer was added. However, the A2's ductility behaviors were different for the two stabilizers. When using the organic stabilizer, as the stabilizer content went up, the ductility of the evaporated residue decreased initially but then climbed up to the peak before it eventually falling sharply. With inorganic stabilizer, as the stabilizer content went up, the ductility of the evaporated residue presented a downward trend.

Zhang, Gao & He (2007) demonstrated that attaining a suitable PH value for the solution may not only enhance the activity of the emulsifier, but also improve the stability of the emulsion, because the PH value can impact the ionization state of the emulsifier. Results showed that as the PH value went up, the ductility was enhanced. This previous study indicated the importance of using ductility as a testing parameter in asphalt property tests. By making comparisons among test samples with different additives, the testing method in this research clearly showed the different effects the additives had on the samples.

The previous papers show the importance of RTFO and DSR test, but none of them mention if the elevation change can affect the RTFO, Ductility and DSR’s test result. The primary purpose of this paper is to find if elevation can affect the test results listed above.

METHODOLOGY

The data used in this paper is taken from round-robin testing organized by the Western Cooperative Test Group board members (WCTG). WCTG was formed in the 1960's with the Wyoming Highway Department Materials Testing Laboratory and several of the asphalt refineries in Wyoming. The Group has since grown to 54 member labs. Most of these are located in the Rocky Mountain area, with the full membership including labs across the continental USA. WCTG is an organization that provides information and assistance to promote mutual understanding between users and producers of asphalt materials. They aim to improve the utilization of standardized testing of asphalt materials. All of the members are volunteers. The purpose of WCTG round-robin binder testing is to provide a continual assessment of existing performance grade (PG) and proposed (PG+) binder grading specifications.

Laboratory tests were conducted by WCTG labs on seven different asphalt binders. There were 19 asphalt suppliers providing asphalt binders for the labs. All the binders went through RTFO aging before being used in the lab tests. Properties measured were the complex modulus (G*); the phase angle, δ; the rutting factor (G*/sin δ); G* at -6C, phase angle at -6C; G*/sin δ at -6C; and ductility. G*, δ, and G*/sin δ were measured at two different temperatures. One temperature was the standard temperature for the test and the second was -6C below this temperature. The purpose of this study was to see if those test results were being impacted by the elevation of the laboratories conducting the tests. One potential reason for the elevation impact may come from differing air density levels.

ANALYSIS

Data sheets were created based on the data from the Western Cooperative Test Group. Seven test parameters from the WCTG database were analyzed. There were 73 labs that volunteered to conduct the RTFO, DSR and Ductility test and build the data pool. These parameters measured were G*, δ, G*/sin δ, G* -6C, δ -6C, G*/sin δ -6C and ductility. G* represents the test result of the complex modulus, δ represents the test result of the phase angle, and G*/sin δ represents the rutting factor.

There were seven different grades of binder specimens: PG 64-22, PG 64-28, PG 64-34, PG 70-22, PG 70-28, PG 76-22 and PG 76-28 (see Table 1). These asphalt binders are commonly used throughout the states.

Procedure

1. Since the purpose of this analysis was to see if there was an effect on the dependent variable with respect to elevation, each dependent variable has been regressed against elevation.
2. For instance: in Figure 2: Complex Modulus Fit Plot PG64-34 shows the Fit Plot for PG64-34, the light blue area is the confidence interval, this means there is 95% confidence that the value of G* at a specified elevation lies within it. In the middle of the blue area, the space is relatively narrower than the right and left hand sides. This means the G* value is closer to the G* actual value in this area than the rest of the blue area. The sample table and graphs are shown below. The rest of the tables and figures on analyzing the G*, δ, G*/sin δ, G*-6C, δ-6C, G*/sin δ -6C and ductility are listed in the Appendix A to G.

Table 1: The Data Set of Complex Modulus (G*)

Elevation Group(ft.)	Elevation (ft.)	LAB No.	PG 64-22	PG 64-28	PG 64-34	PG 70-22	PG 70-28	PG 76-22	PG 76-28
0-500	21	39	3.66	2.83	3.35	3.53	2.87	2.38	2.87
	27	11	3.45	2.91	3.56	3.3	3.42	2.7	2.73
	37	52		2.98	3.54	2.54	2.96	2.59	3
	38	13	3.27	2.83	3.14	3.09	2.72	2.47	2.73
	47	69	3.51	2.51	3.65	3.92	2.88	2.94	3.39
	52	76		2.6	3.39	2.82	3.19		2.29
	78	31	3.13	2.34	3.06	2.96	2.74	2.34	2.8
	194	37	3.59	2.45	3.44	3.07	2.79		2.74
	196	73							
	355	55	3.86	2.79	3.55	2.93	3.33		3.12
	466	83							
	500	65	3.29	2.68				2.67	
501-1000	568	68	3.69				2.43		3.84
	615	64	3.86	2.92	3.78	3.4	3	2.66	3.43
	826	63	3.97	2.85	3.39	2.66	2.91	2.62	3.23
	879	71		3.18		4.08		2.91	3.27
1001-1500	1077	1	3.99	2.83	3.95	3.27	2.9	3.01	3.43
	1084	32	3.63	2.91	3.76	6.28	3.02	2.7	3.25
	1095	81							
	1127	56	3.20	2.68	3.26	3.13	2.65	2.69	2.93
	1135	23		2.46		4.43		2.7	3.35
	1185	24	3.96	2.97	3.63	3.23	2.98	2.85	3.27
1501-2000	1678	26	3.43	2.67	3.21	3.59	2.81	2.42	2.92
	1974	59	3.41	2.82	3.12	2.46	2.71	2.27	2.85
2001-2500	2111	75			3.18				2.82
	2244	3		3.08		2.71		2.57	2.45
	2333	66	3.08		2.8	3.32	3.05	2.37	2.38
	2458	77			3.58	3	3.27		2.56
2501-3000	2523	17	3.11	3.12	3.25	3.41	2.83	2.39	2.84
	2535	78							
	2583	74							
	2673	18	3.28	2.59	3.01	1.89	2.62	2.41	2.5
	2902	4	3.65						

Table 1: The Data Set of Complex Modulus (G*)-continued

Elevation Group(ft.)	Elevation (ft.)	LAB No.	PG 64-22	PG 64-28	PG 64-34	PG 70-22	PG 70-28	PG 76-22	PG 76-28
3001-3500	3103	14		2.76	3.27	3.02	2.76	2.52	3.06
	3187	50		2.68			2.23		2.6
	3258	80							
	3349	22	2.99	2.55	3.26	2.51	2.79	2.24	2.92
	3380	60							
3501-4000	3507	42	3.59	2.69		3.26	2.74	2.55	2.85
	3632	79							
	3879	49	3.36	2.58	3.03	3.32	2.59	2.46	2.9
4001-4500	4028	21	3.02	2.71	3.16	3.49	3.05	2.73	2.89
	4157	35	3.41	2.7	3.02	2.58	2.58	2.47	2.69
	4267	19	3.63	2.88	3.14	3.96	2.82	2.67	3.29
	4294	2	3.08	2.65	3.1	3.53	2.74	2.5	2.74
	4342	38	3.48	2.74	3.19	2.32	2.68	2.07	2.45
	4342	30	3.48	2.78	3.25	3.26	2.25	2.41	2.73
4501-5000	4568	45	3.41	2.6	3.24	2.63	2.96	2.29	2.76
	4657	5	3.09	2.89	3.36	2.67	2.79	2.31	2.86
	4665	46	3.39	2.86	3.04	2.55	2.52	2.64	3.12
	4872	82							
	4882	10	3.13	2.53	2.9	2.45	2.6	2.36	2.62
	4987	57		2.62					2.23
5001-5500	5153	8		2.5	3.07	3.29	2.7	2.39	2.81
	5240	72	3.32	2.46	2.98	2.87	2.66	1.85	3.11
	5445	6	3.20	2.54	3.17	2.8	2.69		2.83
5501-6000	5555	16	3.26	2.83	3.29	3.07	2.79	2.64	3.26
	5613	15	3.74					2.67	
	5971	47		2.46	3.51	3.05	2.85	2.54	2.97
6001-6500	6178	40	3.22	2.68	3.32	2.82	2.73	2.57	2.87
6501-7000	6588	33	3.31	2.64	3.06	3.46	2.05	2.57	2.97
	6798	41	3.19	3.27	3.18	2.78	2.94	2.3	2.65
	6901	25	3.43			3		2.31	

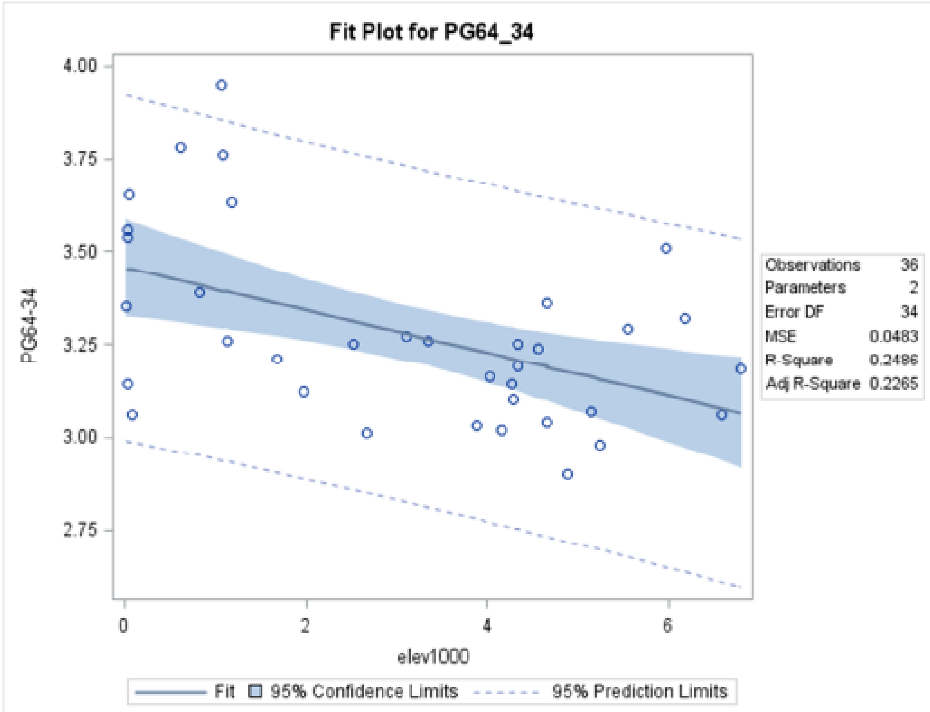

Figure 2: Complex Modulus Fit Plot PG64-34

Table 2: Test Results for Complex Modulus (G*)-PG64-34

PG64-34

Analysis of Variance					
Source	**DF**	**Sum of Squares**	**Mean Square**	**F Value**	**Pr > F**
Model	1	0.54374	0.54374	11.25	0.0020
Error	34	1.64369	0.04834		
Corrected Total	35	2.18743			

Parameter Estimates						
Variable	**Label**	**DF**	**Parameter Estimate**	**Standard Error**	**t Value**	**Pr > |t|**
Intercept	Intercept	**1**	3.45614	0.06438	53.68	<.0001
elev1000		**1**	-0.05756	0.01716	-3.35	0.0020

Regarding interpretation of the regression line for G*/sin δ for Binder PG64-34, all 43 samples were plotted with X as elevation and Y as G*. The regression model is Y_i=$\beta_1 X_i$+β_0+ϵ_i. This model shows the least-squares estimators for making statistical inference. Y_i is the G*. β_1 is the slope, which is the true value of the actual relationship between elevation and sample properties. X_i is the elevation. β_0 is the intercept, which is the expected value of G* when the elevation is zero. ϵ_i is a random variable. This value is subject to variations due to chance. A line Y=$\widehat{\beta_1}$X+$\widehat{\beta_0}$ can be achieved from the plot. $\widehat{\beta_1}$ is the estimator of β_1, $\widehat{\beta_0}$ is the estimator of β_0. X means the elevation and the Y is the G*/sin δ. For instance, in the Table 1 for binder PG64-34, $\widehat{\beta_0}$ is 3.45614, $\widehat{\beta_1}$ is -0.05756, alpha is 0.05. If the P-value is smaller than 0.05, then the slope is not zero at an α=0.05 confidence level. If the P-value is bigger than 0.05, then the slope is zero at a α=0.05 confidence level. This indicates as elevation goes up, G* does not present significant change.

Table 3 is a summary of regression analysis for G*, δ, G*/sin δ, G* -6C, δ -6C, G*/sin δ -6C and ductility. The shaded area in Table 3 indicates the binders and parameters that were affected by elevation at approximately α = 0.05. The rest of the analysis tables and figures are in the Appendix sections. Appendix A includes tables and figures for G*, Appendix B includes tables and figures for δ, Appendix C includes tables and figures for G*/sin δ, Appendix D is for G* -6C, Appendix E is for δ -6C, Appendix F is for G*/sin δ -6C and Appendix G is for Ductility.

Table 3. Summary of Regression Analysis for All WCTG Data

		Binder								
Dependent Variable		64-22	64-28	64-34	70-22	70-28	76-22	76-28	Avg	s
G*	P > F	0.009	0.400	0.002	0.170	0.005	0.027	0.100		
	Slope	-0.058		-0.057		-0.049	-0.039		-0.050	0.009
δ	P > F	0.006	0.029	0.070	0.340	0.004	0.094	0.037		
	Slope	0.097		0.155		0.127	0.111	0.158	0.130	0.027
G* / sin δ	P > F	0.017	0.077	0.007	0.208	0.278	0.030	0.014		
	Slope	-0.056	-0.060	-0.083			-0.054	-0.077	-0.066	0.013
G* -6C	P > F		0.158	0.002	0.171	0.072	0.022	0.098		
	Slope			-0.095		-0.113	-0.051	-0.054	-0.078	0.031
δ −6c	P > F		0.023	0.132	0.394	0.017	0.216	0.078		
	Slope		0.321			0.150		0.114	0.195	0.111
G* / sin δ −6C	P > F		0.014	0.003	0.143	0.143	0.059	0.086		
	Slope		-0.079	-0.131			-0.054	-0.078	-0.086	0.032
Ductility	P > F		0.655	0.050	0.950	0.460	0.596	0.365		
	Slope			1.280						

Analysis of the Table A

The slope of the G* regression line is -0.058, -0.057, -0.049, and -0.039 for the 64-22, 64-34, 70-28 and 76-22 asphalts, respectively. The average of these slopes is -.0050 with a standard deviation of 0.009. This means that the G* value decreases at the rate of -0.048 for each 1000 feet in elevation change from sea level. If a laboratory in Florida at sea level obtains a value for G* of 3.0 kPa, then a laboratory in Santa Fe, NM at 7000 feet above sea level should expect to obtain a value of 7 x -0.048 kPa less than this or 3 kPa – (0.336) = 2.664 kPa.

The slope of the δ regression line is 0.097, 0.155, 0.127, 0.111, 0.158 for the 64-22, 64-34, 70-28, and 76-22 asphalts, respectively. The average of these slopes is 0.13 with a standard deviation of 0.027. This means that the δ value increases at the rate of 0.13 for each 1000 ft. of elevation change from sea level. So, if a lab in Florida at sea level obtains a value for δ of 70 degree, then a lab in Santa Fe, NM at 7000 ft. above sea level should expect to obtain a value of 70+7x0.13=70.91 degree.

The slope of the G*/sin δ regression line is -0.056, -0.060, -0.083, -0.054 and -0.083 for the 64-22, 64-28, 64-34, 76-22 and 76-28 asphalts, respectively. The average of these slopes is -0.066 with a standard deviation of 0.013. This means that the G*/sin δ value decreases at the rate of -0.066 for each 1000 feet in elevation change from sea level. So, if a laboratory in Florida at sea level obtains a value for G*/sin δ of 5.0kPa, then a laboratory in Santa Fe, NM at 7000 feet at sea level should expect a value of 5.0-0.066x7=4.538 kPa.

The slope of the G* - 6C regression line is -0.095, -0.113, -0.051 and -0.054 for the 64-34, 70-28, 76-22 and 76-28 asphalts, respectively. The average of these slopes is -0.078 with a deviation of 0.031. This means that the G* value decreases at the rate of -0.078 for each 1000 feet in elevation change from sea level. So, if a laboratory in Florida at sea level obtains a value for G* of 3.0kPa, then a laboratory in Santa Fe, NM at 7000 feet above sea level should expect to obtain a value of 3-7 x 0.078=2.454kPa.

The slope of the δ regression line is 0.321, 0.15 and 0.114 for the 64-28, 70-28 and 76-28 asphalts, respectively. The average of these slopes is 0.195 with a standard deviation of 0.111. This means that the δ value increases at the rate of 0.195 for each 1000 feet in elevation change from sea level. So, if a laboratory in Florida at sea level obtains a value for δ of 70 degrees, then a laboratory in Santa Fe, NM at 7000 feet above sea level should expect to obtain a value of 70+0.195x7= 71.365 degree.

The slope of the G* regression line is -0.079, -0.131, -0.054 and -0.078 for the 64-28, 64-34, 76-22 and 76-28 asphalts, respectively. The average of these slopes is -0.086 with a standard deviation of -0.086. This means that the G*/sin δ value decreases at the rate of

-0.086 for each 1000 feet in elevation change from sea level. So, if a laboratory in Florida at sea level obtains a value for G* of 3.0kPa, then a laboratory in Santa Fe, NM at 7000 feet above sea level should expect to obtain a value of 3kPa- 7 x0.086=2.398kPa.

CONCLUSIONS

The analysis in the Analysis chapter shows that the parameters G*, δ, G*/sin δ, G*-6C, δ-6C, and G*/sin δ -6C linear trends as elevation goes up. Since only one binder was affected by elevation in the ductility test, it is difficult to conclude that ductility is affected by elevation.

The following parameters and binders were affected by elevation:

G*:	64-22, 64-34, 70-28 and 76-22
δ:	64-22, 64-34, 70-28 and 76-22
G*/sin δ:	64-22, 64-28, 64-34, 76-22 and 76-28.
G*-6C:	64-34, 70-28, 76-22 and 76-28
δ- 6C:	64-28, 70-28 and 76-28
G*/sin δ -6C:	64-28, 64-34, 76-22 and 76-28.

Even though the analysis concluded that elevation can affect the parameters, there may also be other factors that affect the test results. For instance, the daily air pressure might be different due to the weather conditions. If a strong storm comes, the air pressure can drop dramatically, which would cause the oxidative level to decrease. The results of this study indicates that certain binder properties can be affected by the elevation at where the rolling thin film oven test is conducted and the binder properties are measured. Thus, elevation should be considered when conducting DSR tests.

Since not a lot data was collected on the ductility test. The ductility test did not show the test results be influenced by elevation. More data would provide a stronger basis for assessing the effect of elevation on ductility.

The insufficient amount of data is the limitation of this research, but it does show that DSR test results can be affected by elevation change. Overall, the different Performance Grade asphalt sample only present linear regression for certain test parameters. For example, When using PG 64-22 binder for testing, only parameter G*, δ, G*/sin δ are affected, while PG 70-28 works for G*, δ, G*-6C, and δ- 6C. There was a guess that PG 64-22 can possibly present linear regression for parameters G*-6C, δ-6C and G*/sin δ -6C. Thus, the recommendation is that the data providers, Western Cooperative Test Group board members, can keep collecting data for these parameters. Additionally, the next research topic based on this one should see how much the difference the elevation can cause. If the difference is within the tolerance of requirements, then we do not need to adjust the specs. If the difference is beyond the spec's tolerance, then the specs should be adjusted. It is also possible that the neighbor elevations, like 0-1000 f.t. and 1000-2000 f.t., do not present significant difference. But the 0-1000 f.t. differs a lot from 5000-6000 f.t. elevation level.

REFERENCES

Al-Khateeb, G.G., & Al-Akhras, N.M. (2011). Properties of Portland cement-modified asphalt binder using Superpave tests. *Construcction and Building Materials, 25(2),* 926-932.

Anderson, D.A., Christensen, D.W., Dongre, R., Sharma, M.G., & Jordhal P. (1990). Asphalt behavior at low service temperatures. *FHWA Report*. FHWA-RD-88-078.

Asphalt Pavement Alliance. (2013). Asphalt Pavement. *Asphalt Pavement Alliance*.

ASTM Standard (2013). Standard test method for effect of heat and air on a moving film of asphalt (rolling thin-film oven test). *ASTM International*. DOI: 10.1520/D2872-12.

Bahia, H.U. & Anderson, D.A. (1995). The SHRP binder rheological parameters: Why are they required and how do they compare to conventional properties. *Transportation Research Board*, Preprint Paper No. 950793.

Colbert, B., Beale, J. M., & You, Z. (2011). Low temperature cracking potential of aged asphalts using simulated aging techniques*. 11th International Conference of Chinese Transportation Professionals (ICCTP)*. Retrieved from http://ascelibrary.org/doi/abs/10.1061/41186%28421%29410

Daniel, J. S., & Bisirri, W. M. (2005*).* Characterizing fatigue in pavement materials using a dissipated energy parameter. *GSP 130 Advances in Pavement Engineering*. Retrieved from http://ascelibrary.org/doi/pdfplus/10.1061/40776%28155%2916

Epps M.A., Park, E.S., Arambula, E., & Spiegelman, C. (2002*). Assessment of the TxDOT binder quality assurance program.* Rep. No. 4047-2, Texas Transportation Institute: College Station, TX.

Fu, Z., Liu, Z., & Jing, L. (2009). Effect by different factors on ductility of evaporated residue of modified emulsion asphalt. *ICCTP 2009*, 1-6. DOI: 10.1061/41064(358)297.

Gandhi,T., Akisetty, C., & Amirkhanian, S. (2010). A comparison of warm asphalt binder aging with laboratory aging procedures. *American Society of Testing and Materials, USA, 38*. DOI: 10.1520/JTE101934.

Goodrich, J.L. (1991). Asphalt binder theology, asphalt concrete rheology and asphalt concrete mix properties. *Journal of the Association of Asphalt Paving Technologists*, *60*, 80-120.

History of asphalt. (2013). *National Asphalt Pavement Association*. Retrieved from https://www.asphaltpavement.org/index.php?option=com_content&view=article&id=21&Itemid=41

Jemison, H.B., Burr, B.L., Davison, R.R., Bullin, J.A., & Glover, C.J. (1992). Application and use of the ATR, FT-IR method to asphalt aging studies. *Fuel Sci. Technol. Int.*, *10,* 795-808.

Mercado, E.A., Martin, A.E., Park, E.S., Spiegelman,C. & Glover, C.J. (2005). Factors affecting binder properties between production and construction. *American Society of Engineers*. DOI: 10.1061/(ASCE)0899-1561(2005)17:1(89).

Mushrush, G.W. & Speight, J.G. (1995). *Petroleum products: Instability and incompatibility*. Taylor & Francis: Washington, DC.

Pauli, A.T., & Huang, S.C. (1997). Relationship between asphalt compatibility, flow properties, and oxidative aging. *Chinese Society of Pavement Engineering, 6(1),* 1-7.

Pavement Interactive. (2008). Retrieved from http://www.pavementinteractive.org/article/rutting/

Pavement Interactive. (2009). Retrieved from http://www.pavementinteractive.org/article/fatigue-cracking/

Pavement Interactive. (2011). Retrieved from http://www.pavementinteractive.org/article/dynamic-shear-rheometer/

Roberts, F.L., Kandhal, P.S., Brown, E.R., Lee, D.Y., & Kennedy, T.W. (1996). *Hot mix asphalt materials, mixture design, and construction*. Lanham, MD: NAPA Research and Education Foundation.

Ksaibati,K., & Stephen, J. (1999). Utilization of bottom ash in asphalt mixes. *Upper Great Plains Transportation Institute.*

Standard terminology relating to roofing and waterproofing. (2013). Retrieved from http://enterprise2.astm.org/DOWNLOAD/D1079.1378908-1.pdf

Zhang, J., Gao, S., & He, Z. (2007). The performance effect of chemical modification to emulsified SBR modified emulsified asphalt. *Petroleum Asphalt, 21(3),* 24-27.

Zhou, L., Li, P., & Zhang, Z. (2009). Investigation of high temperature properties of asphalt mixture containing fibers. *Material Design, Construction, Maintenance, and Testing of Pavements,* 139-144.

Zirlin, J. (2009). Bringing innovations to market. *Public Roads, 72 (4)*.
Retrieved from http://ascelibrary.org/doi/abs/10.1061/41186%28421%29410

APPENDIX A: REGRESSION ANALYSIS OF THE DATA SET OF COMPLEX MODULUS (G*)

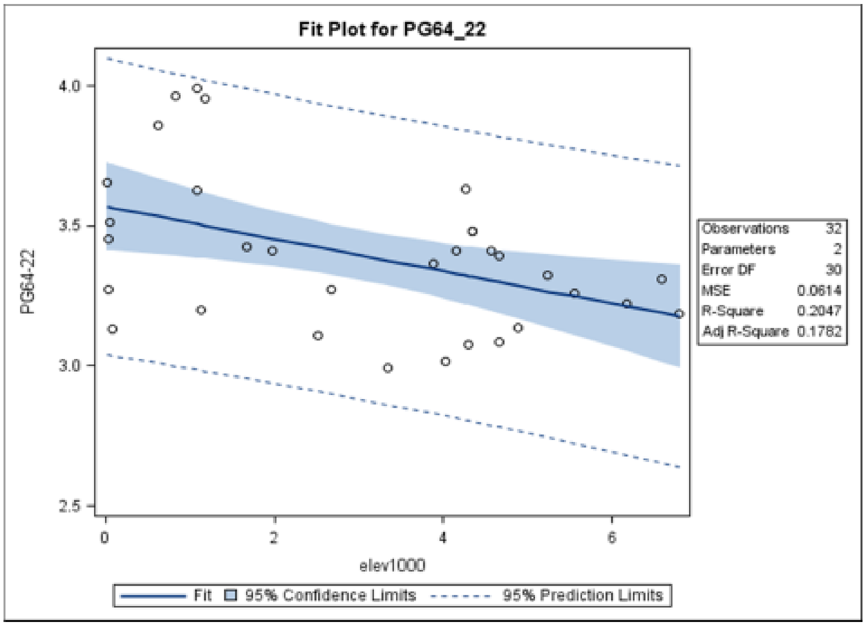

Figure 3: Complex Modulus Fit Plot PG64-22

Table 4: Test Results for Complex Modulus-PG64-22

PG64-22

Analysis of Variance					
Source	**DF**	**Sum of Squares**	**Mean Square**	**F Value**	**Pr > F**
Model	1	0.47395	0.47395	7.72	0.0093
Error	30	1.84153	0.06138		
Corrected Total	31	2.31548			

Parameter Estimates						
Variable	**Label**	**DF**	**Parameter Estimate**	**Standard Error**	**t Value**	**Pr > |t|**
Intercept	Intercept	**1**	3.56942	0.07661	46.59	<.0001

Parameter Estimates						
Variable	**Label**	**DF**	**Parameter Estimate**	**Standard Error**	**t Value**	**Pr > |t|**
elev1000		**1**	-0.05776	0.02079	-2.78	0.0093

Table 5: Test Results for Complex Modulus-PG64-28

Test Results for Complex Modulus-PG64-28

PG64-28

Analysis of Variance					
Source	**DF**	**Sum of Squares**	**Mean Square**	**F Value**	**Pr > F**
Model	1	0.02763	0.02763	0.71	0.4038
Error	34	1.31466	0.03867		
Corrected Total	35	1.34230			

Parameter Estimates						
Variable	**Label**	**DF**	**Parameter Estimate**	**Standard Error**	**t Value**	**Pr > |t|**
Intercept	Intercept	**1**	2.78530	0.05758	48.37	<.0001
elev1000		**1**	-0.01298	0.01535	-0.85	0.4038

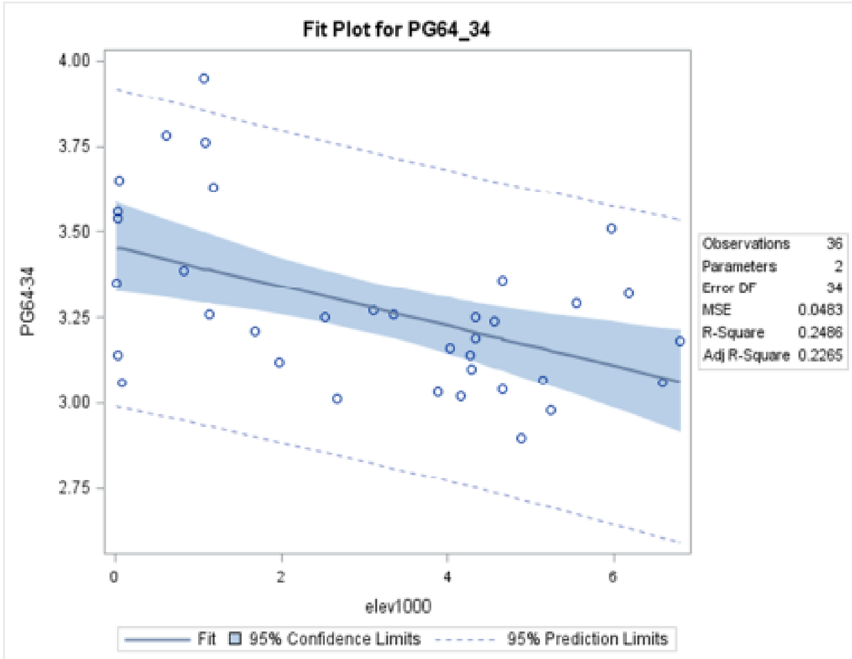

Figure 4: Complex Modulus Fit Plot PG64-34

Table 6: Test Results for Complex Modulus-PG64-34

PG64-34

Analysis of Variance					
Source	**DF**	**Sum of Squares**	**Mean Square**	**F Value**	**Pr > F**
Model	1	0.54374	0.54374	11.25	0.0020
Error	34	1.64369	0.04834		
Corrected Total	35	2.18743			

Parameter Estimates						
Variable	**Label**	**DF**	**Parameter Estimate**	**Standard Error**	**t Value**	**Pr > |t|**
Intercept	Intercept	**1**	3.45614	0.06438	53.68	<.0001
elev1000		**1**	-0.05756	0.01716	-3.35	0.0020

Table 7: Test Results for Complex Modulus-PG70-22

PG70-22

Analysis of Variance					
Source	**DF**	**Sum of Squares**	**Mean Square**	**F Value**	**Pr > F**
Model	1	0.96934	0.96934	1.96	0.1706
Error	34	16.81814	0.49465		
Corrected Total	35	17.78747			

Parameter Estimates						
Variable	**Label**	**DF**	**Parameter Estimate**	**Standard Error**	**t Value**	**Pr > |t|**
Intercept	Intercept	**1**	3.35620	0.20594	16.30	<.0001
elev1000		**1**	-0.07686	0.05490	-1.40	0.1706

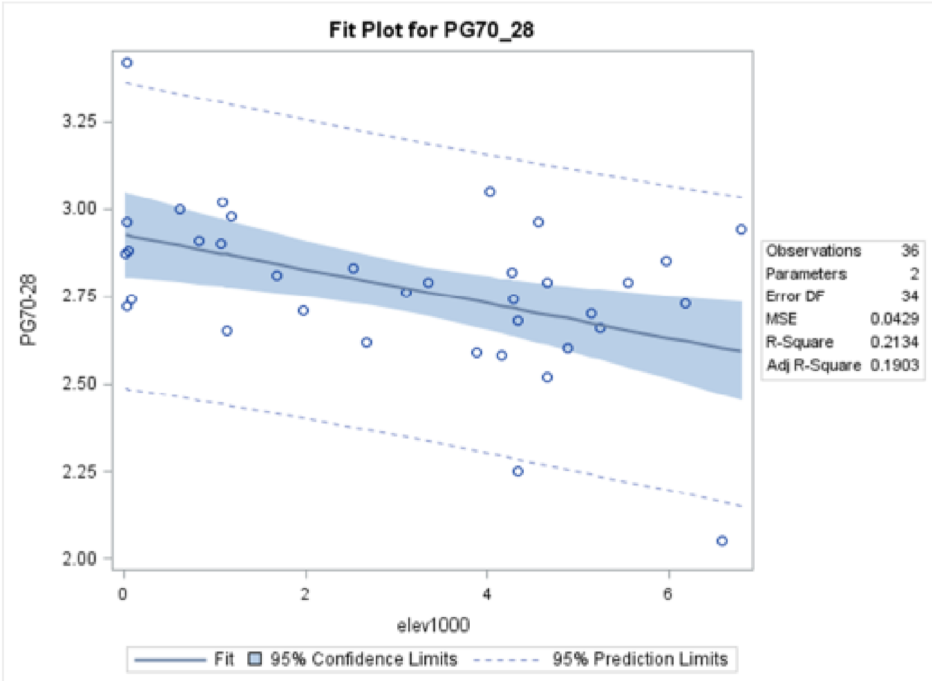

Figure 5: Complex Modulus Fit Plot PG70-28

Table 8: Test Results for Complex Modulus-PG70-28

PG70-28

Analysis of Variance

Source	DF	Sum of Squares	Mean Square	F Value	Pr > F
Model	1	0.39596	0.39596	9.23	0.0046
Error	34	1.45911	0.04292		
Corrected Total	35	1.85507			

Parameter Estimates

Variable	Label	DF	Parameter Estimate	Standard Error	t Value	Pr > |t|
Intercept	Intercept	**1**	2.92566	0.06066	48.23	<.0001
elev1000		**1**	-0.04912	0.01617	-3.04	0.0046

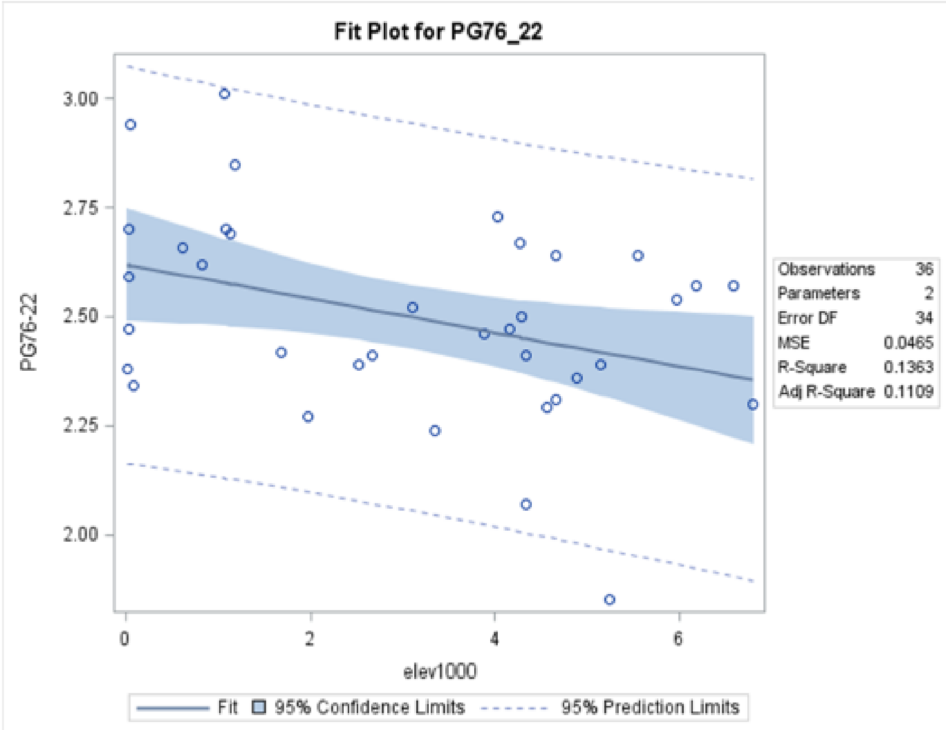

Figure 6: Complex Modulus Fit Plot PG76-22

Table 9: Test Results for Complex Modulus-PG76-22

PG76-22

Analysis of Variance

Source	DF	Sum of Squares	Mean Square	F Value	Pr > F
Model	1	0.24956	0.24956	5.37	0.0267
Error	34	1.58151	0.04652		
Corrected Total	35	1.83107			

Parameter Estimates

Variable	Label	DF	Parameter Estimate	Standard Error	t Value	Pr > |t|
Intercept	Intercept	1	2.61944	0.06315	41.48	<.0001
elev1000		1	-0.03900	0.01684	-2.32	0.0267

Table 10: Test Results for Complex Modulus-PG76-28

PG76-28

Analysis of Variance					
Source	**DF**	**Sum of Squares**	**Mean Square**	**F Value**	**Pr > F**
Model	1	0.17111	0.17111	2.81	0.1028
Error	34	2.06989	0.06088		
Corrected Total	35	2.24100			

Parameter Estimates						
Variable	**Label**	**DF**	**Parameter Estimate**	**Standard Error**	**t Value**	**Pr > |t|**
Intercept	Intercept	**1**	3.03959	0.07225	42.07	<.0001
elev1000		**1**	-0.03229	0.01926	-1.68	0.1028

APPENDIX B: ANALYSIS OF THE DATA SET FOR PHASE ANGLE (Δ)

Table 11: The Data Set of Phase Angle (δ)

Elevation Group(ft.)	Elevation (ft.)	LAB No.	PG 64-22	PG 64-28	PG 64-34	PG 70-22	PG 70-28	PG 76-22	PG 76-28
0-500	21	39	84.1	67.5	55	66.98	65.25	60.1	58.87
	27	11	84.3	67.43	54.75	68.4	64.3	60.4	57.64
	37	52		65.5	50.8	71.45	64.95	60.3	58.6
	38	13	84.4	66.35	55.35	69.3	66.05	60.5	60.3
	47	69	84.2	66.3	55.55	68.6	64.75	60.3	58
	52	76		72.8	52	72.4	64.9		63.1
	78	31	83.9	71	55.3	69.33	65.2	59.85	58.03
	194	37	84	69.35	54.8	68.8	65.25		58.87
	196	73							
	355	55	83.55	65.45	54.5	67.63	63.6		57.75
	466	83							
	500	65	84.4	65				61.4	
501-1000	568	68	83.8				66.2		57.9
	615	64	83.8	67.3	51	66.28	64.85	59	55.8
	826	63	83.7	67.9	54.65	71.15	65.25	60	57.88
	879	71		64.35		65.1		58.9	56.3
1001-1500	1077	1	83.85	67.83	54.9	69.58	65.05	59.55	57.83
	1084	32	84	64.8	50.7	63.3	64.6		56.6
	1095	81							
	1127	56	84.7	68.03	55.05	69.1	65.95	60.45	58.48
	1135	23		65.1		68.6		61.4	56.5
	1185	24	83.7	67.67	51.5	68.45	65.15	59.2	58.73
1501-2000	1678	26	84.25	68.43	54.85	66.7	65.25	60.4	58.5
	1974	59	84.4	69.6	54.5	72.2	65.65	60.75	59.05
2001-2500	2111	75			52				58.2
	2244	3		66.3		65.7		59.3	56.4
	2333	66	84.95		55.55	67.3	65.4	60.2	56.5
	2458	77			51.8	70.5	63.6		64.4
2501-3000	2523	17	84.85	69.5	54.7	69.4	65.95	61.55	59.15
	2535	78							
	2583	74							
	2673	18	84.6	66.25	55.15	71.75	65.9	60.05	59.28
	2902	4	84.6						

Table 11: The Data Set of Phase Angle (δ)-continued

3001-3500	3103	14		68.63	55.4	67.7	65.95	60.65	58.83
	3187	50		73.1			67.2		61.9
	3258	80							
	3349	22	84.5	68.35	55.65	68.53	65.1	62.6	61
	3380	60							
3501-4000	3507	42	84.3	68.23		67.17	65.25	59.2	58.87
	3632	79							
	3879	49	84.35	68.55	55.7	71.37	65.3	61.1	59.4
4001-4500	4028	21	84.8	72.9	55.4	67.15	65.35	60.4	58.8
	4157	35	84	68.17	55.95	68.67	66.15	60.45	59.65
	4267	19	84.3	65.5	55.65	62.95	65.95	58.7	59.93
	4294	2	84.8	68.13	54.9	65.83	65.75	60.35	58.88
	4342	38	84.55	68.77	55.2	72.1	65.95	60.6	59.85
	4342	30	84.55	68.1	54.85	67.63	67.1	60.4	59.97
4501-5000	4568	45	84.2	67.67	54.65	74.63	65.5	60.9	59.3
	4657	5	84.8	65.3	54.9	66.95	65.65	60.9	59.17
	4665	46	84.3	69	55	69.27	65.55	60.5	59.28
	4872	82							
	4882	10	84.4	68.37	56.3	66.25	65.95	59.1	59.18
	4987	57		66.5					59.3
5001-5500	5153	8	84.3	68.57	55.35	67.43	65.65	60.7	59.08
	5240	72	84.8	69	56.2	72.57	66.1	62	58.9
	5445	6	84.55	69.07	52.7	69.93	66.1		59.17
5501-6000	5555	16	83.9	68.07	54.85	72.73	65.05	61.3	58.7
	5613	15						58.6	
	5971	47	86.1	68.7	55	69.25	65.55	60.1	58.6
6001-6500	6178	40	84.4	67.93	54.7	69.83	65.35	60.25	58.68
6501-7000	6588	33	84.5	68.3	55.45	73.6	67	60.45	57.9
	6798	41	84.65	70.15	54.85	68.73	65.7	61.2	59.68
	6901	25				67.8		60.8	

Delta Regression Analysis

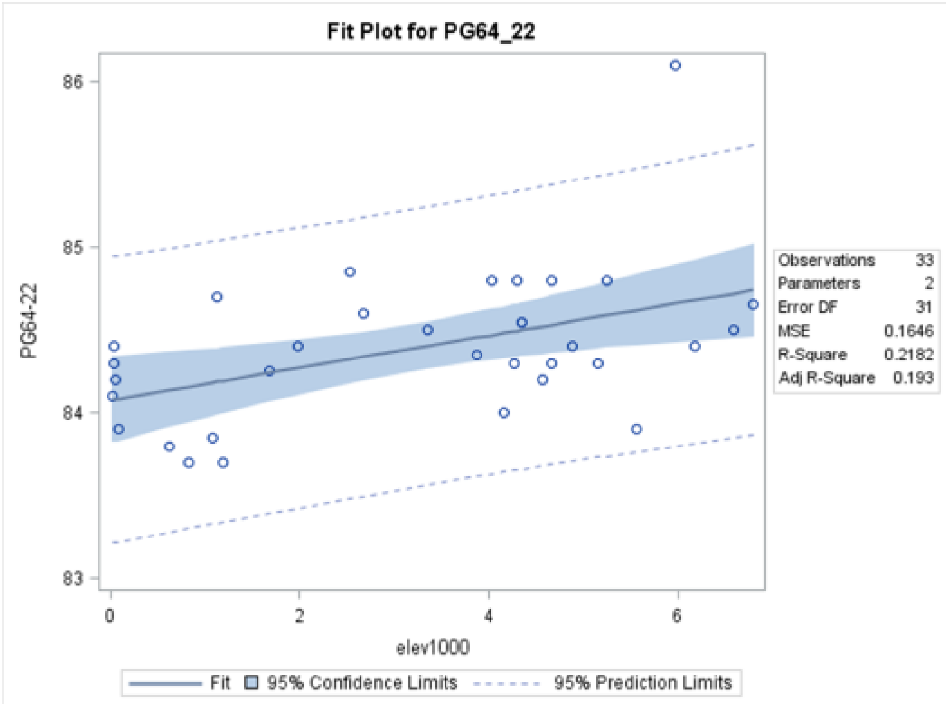

Figure 7: Phase Angle Fit Plot PG64-22

Table 12: Test Results for Phase Angle-PG64-22

PG64-22

Analysis of Variance					
Source	**DF**	**Sum of Squares**	**Mean Square**	**F Value**	**Pr > F**
Model	1	1.42389	1.42389	8.65	0.0061
Error	31	5.10171	0.16457		
Corrected Total	32	6.52561			

Parameter Estimates						
Variable	**Label**	**DF**	**Parameter Estimate**	**Standard Error**	**t Value**	**Pr > |t|**
Intercept	Intercept	**1**	84.07715	0.12836	655.03	<.0001
elev1000		**1**	0.09742	0.03312	2.94	0.0061

Table 13: Test Results for Phase Angle-PG64-28

PG64-28

Analysis of Variance

Source	DF	Sum of Squares	Mean Square	F Value	Pr > F
Model	1	2.47911	2.47911	1.16	0.2906
Error	31	66.48308	2.14462		
Corrected Total	32	68.96219			

Parameter Estimates

Variable	Label	DF	Parameter Estimate	Standard Error	t Value	Pr > |t|
Intercept	Intercept	**1**	67.78460	0.46336	146.29	<.0001
elev1000		**1**	0.12854	0.11955	1.08	0.2906

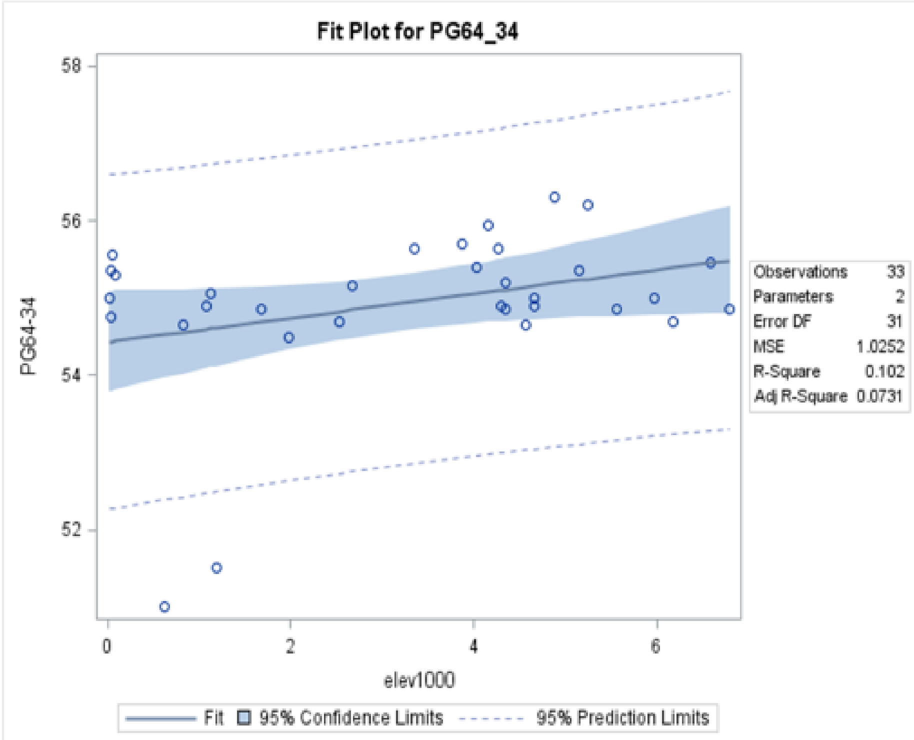

Figure 8: Phase Angle Fit Plot PG64-34

Table 14: Test Results for Phase Angle-PG64-34

PG64-34

Analysis of Variance					
Source	**DF**	**Sum of Squares**	**Mean Square**	**F Value**	**Pr > F**
Model	1	3.61163	3.61163	3.52	0.0700
Error	31	31.78170	1.02522		
Corrected Total	32	35.39333			

Parameter Estimates						
Variable	**Label**	**DF**	**Parameter Estimate**	**Standard Error**	**t Value**	**Pr > |t|**
Intercept	Intercept	**1**	54.43122	0.32037	169.90	<.0001
elev1000		**1**	0.15515	0.08266	1.88	0.0700

Table 15: Test Results for Phase Angle-PG70-22

PG70-22

Analysis of Variance					
Source	**DF**	**Sum of Squares**	**Mean Square**	**F Value**	**Pr > F**
Model	1	5.94313	5.94313	0.94	0.3397
Error	31	195.94668	6.32086		
Corrected Total	32	201.88981			

Parameter Estimates						
Variable	**Label**	**DF**	**Parameter Estimate**	**Standard Error**	**t Value**	**Pr > |t|**
Intercept	Intercept	**1**	68.52831	0.79548	86.15	<.0001
elev1000		**1**	0.19902	0.20525	0.97	0.3397

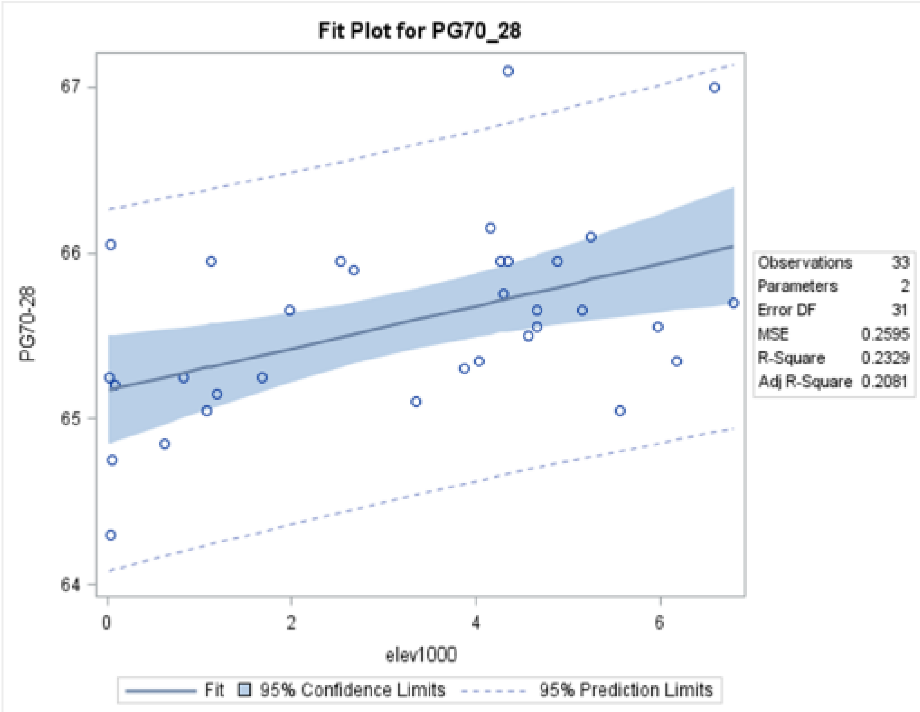

Figure 9: Phase Angle Fit Plot PG70-28

Table 16: Test Results for Phase Angle-PG70-28

PG70-28

Analysis of Variance					
Source	**DF**	**Sum of Squares**	**Mean Square**	**F Value**	**Pr > F**
Model	1	2.44244	2.44244	9.41	0.0045
Error	31	8.04589	0.25954		
Corrected Total	32	10.48833			

Parameter Estimates						
Variable	**Label**	**DF**	**Parameter Estimate**	**Standard Error**	**t Value**	**Pr > |t|**
Intercept	Intercept	**1**	65.17041	0.16119	404.30	<.0001
elev1000		**1**	0.12759	0.04159	3.07	0.0045

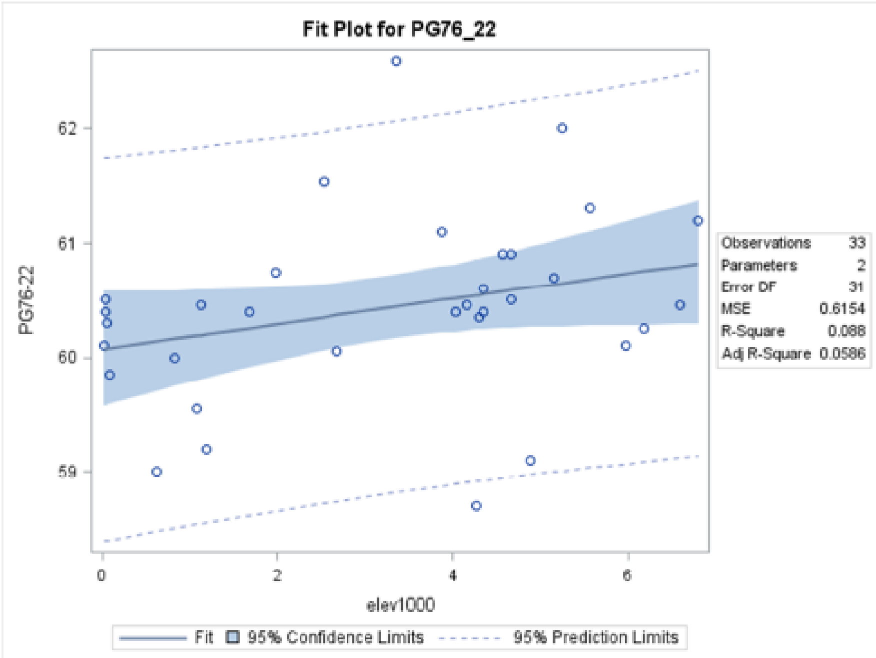

Figure 10: Phase Angle Fit Plot PG76-22

Table 17: Test Results for Phase Angle-PG76-22

PG76-22

Analysis of Variance					
Source	**DF**	**Sum of Squares**	**Mean Square**	**F Value**	**Pr > F**
Model	1	1.84177	1.84177	2.99	0.0936
Error	31	19.07869	0.61544		
Corrected Total	32	20.92045			

Parameter Estimates						
Variable	**Label**	**DF**	**Parameter Estimate**	**Standard Error**	**t Value**	**Pr > |t|**
Intercept	Intercept	**1**	60.06871	0.24822	242.00	<.0001
elev1000		**1**	0.11079	0.06404	1.73	0.0936

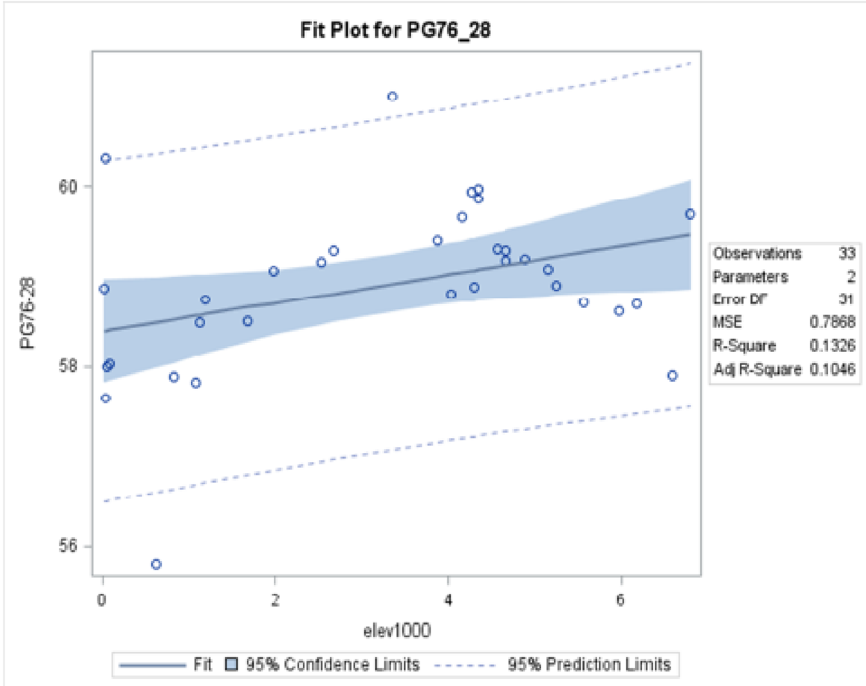

Figure 11: Phase Angle Fit Plot PG76-28

Table 18: Test Results for Phase Angle-PG76-28

PG76-28

Analysis of Variance					
Source	**DF**	**Sum of Squares**	**Mean Square**	**F Value**	**Pr > F**
Model	1	3.72935	3.72935	4.74	0.0372
Error	31	24.39081	0.78680		
Corrected Total	32	28.12016			

Parameter Estimates						
Variable	**Label**	**DF**	**Parameter Estimate**	**Standard Error**	**t Value**	**Pr > |t|**
Intercept	Intercept	**1**	58.38340	0.28066	208.03	<.0001
elev1000		**1**	0.15765	0.07241	2.18	0.0372

APPENDIX C: REGRESSION ANALYSIS OF THE DATA SET FOR G*/SIN Δ

Table 19: The Data Set of G*/sin δ

Elevation Group(ft.)	Elevation (ft.)	LAB No.	PG 64-22	PG 64-28	PG 64-34	PG 70-22	PG 70-28	PG 76-22	PG 76-28
0-500	21	39	3.68	5.58	4.07	2.96	4.25	2.75	3.36
	27	11	3.47	5.42		2.92	4.04	2.97	3.33
	37	52		5.95	4.56	2.71	3.83	2.98	3.52
	38	13	3.29	5.76	3.84	3.31	3.38	2.84	3.15
	47	69	3.53	4.9	4.42	3.82	4.2	3.38	4.02
	52	76		5.32	4.31	2.96	3.52		2.57
	78	31	3.15	4.81	3.73	3.17	3.96	2.71	3.32
	194	37	3.61	4.9	4.23	3.31	4		3.22
	196	73							
	355	55	3.89	5.42	4.37	3.18	3.72		3.7
	466	83							
	500	65	3.31	5.2				3.04	
501-1000	568	68	3.71						4.53
	615	64	3.88	5.98	4.82	3.76	3.93	3.1	4.16
	826	63	3.99	5.79	4.19	2.82	4.25	3.03	3.83
	879	71		6.46		4.56		3.4	3.92
1001-1500	1077	1	4.02	5.93	4.85	3.48	4.56	3.49	4.1
	1084	32	3.65	5.71	4.86	7.03	4.4	2.92	3.89
	1095	81							
	1127	56	3.22	5.06	3.99	3.36	3.71	3.1	3.44
	1135	23		4.7		4.88		3.08	4.01
	1185	24	3.98	5.88	4.64	3.48	4.36	3.31	3.89
1501-2000	1678	26	3.45	5.35	3.94	3.98	4.17	2.78	3.43
	1974	59	3.43	5.22	3.83	2.62	3.33	2.61	3.32
2001-2500	2111	75			4.04				3.3
	2244	3		6.08		2.97		2.99	2.94
	2333	66	3.1		3.45	3.65	3.36	2.73	2.86
	2458	77			4.56	3.19	3.65		2.76
2501-3000	2523	17	3.12	5.95	4	3.65	3.43	2.72	3.32
	2535	78							
	2583	74							
	2673	18	3.29	5.74	3.68	2.05	3.13	2.78	2.91
	2902	4	3.67						

Table 19: The Data Set of G*/sin δ-continued

3001-3500	3103	14		5.8	3.98	3.26	3.38	2.9	3.58
	3187	50							2.95
	3258	80							
	3349	22	3.01		3.26	2.6	3.39	2.24	3.01
	3380	60							
3501-4000	3507	42	3.61	5.97	4.37	3.56	3.79	3.12	3.22
	3632	79							
	3879	49	3.38	4.98	3.69	3.52	3.89	2.81	3.38
4001-4500	4028	21	3.03	4.89	3.87	3.86	4.4	3.13	3.39
	4157	35	3.43	5.44	3.68	2.79	3.76	2.85	3.1
	4267	19	3.65	5.67	3.81	4.45	3.35	3.12	3.8
	4294	2	3.09	5.23	3.81	3.92	3.38	2.88	3.2
	4342	38	3.5	5.45	4.01	3.57	4.66	2.78	2.66
	4342	30	3.5	5.45	3.91	2.47	3.79	2.37	2.84
4501-5000	4568	45	3.43	5.34	4	2.72	3.88	2.62	3.21
	4657	5	3.1	5.59	4.11	2.9	4.05	2.64	3.35
	4665	46	3.41	5.78	3.73	2.74	3.75	3.03	3.65
	4872	82							
	4882	10	3.15	4.95	3.51	2.67	3.77	2.75	3.07
	4987	57		5.45					2.62
5001-5500	5153	8	3.34	5.15	3.76	3.61	4	2.75	3.28
	5240	72	3.21	4.83	3.62	3.01	3.86	2.09	3.65
	5445	6	3.28	5.08	3.99	2.98	3.4		3.31
5501-6000	5555	16	3.77		4.04	3.22	3.51	3.01	3.84
	5613	15						3.12	
	5971	47	3.23	4.86	3.98	3.28	3.89	2.93	3.49
6001-6500	6178	40	3.33	5.13	4.08	3.01	3.99	2.96	3.37
6501-7000	6588	33	3.2	6.15	3.74		3.81	2.95	3.5
	6798	41	3.44	5.28	3.91	3	3.57	2.63	3.08
	6901	25				3.23		2.64	

G* / sin δ

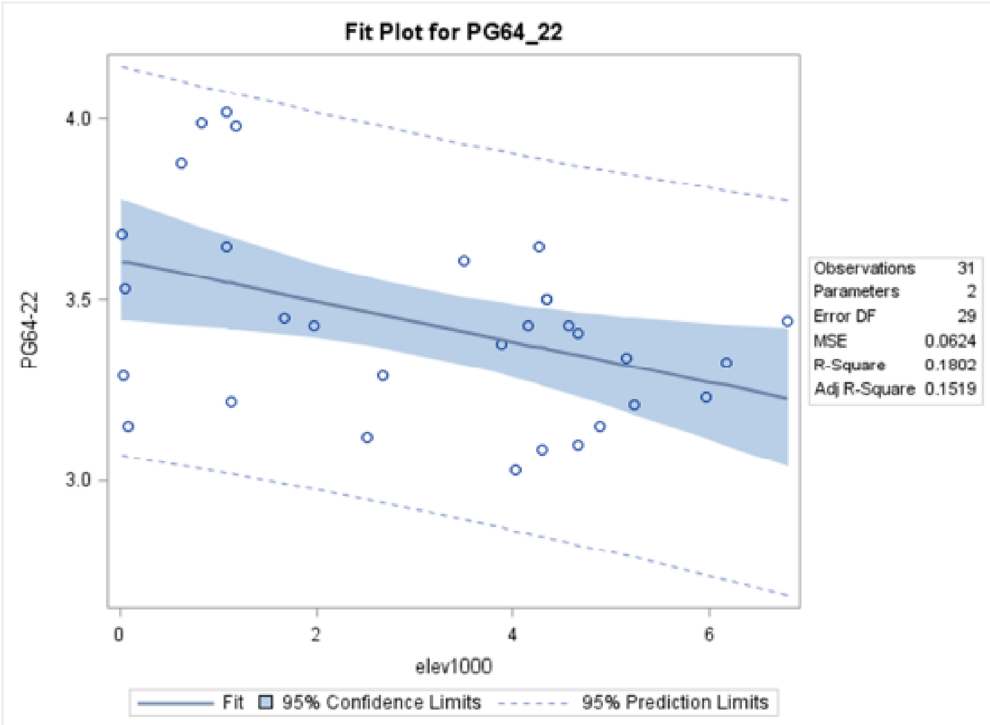

Figure 12: G* / sin δ Fit Plot PG64-22

Table 20: Test Results for G* / sin δ-PG64-22

PG64-22

Analysis of Variance					
Source	**DF**	**Sum of Squares**	**Mean Square**	**F Value**	**Pr > F**
Model	1	0.39782	0.39782	6.37	0.0173
Error	29	1.80993	0.06241		
Corrected Total	30	2.20775			

Parameter Estimates						
Variable	**Label**	**DF**	**Parameter Estimate**	**Standard Error**	**t Value**	**Pr > |t|**
Intercept	Intercept	**1**	3.60877	0.08189	44.07	<.0001
elev1000		**1**	-0.05593	0.02215	-2.52	0.0173

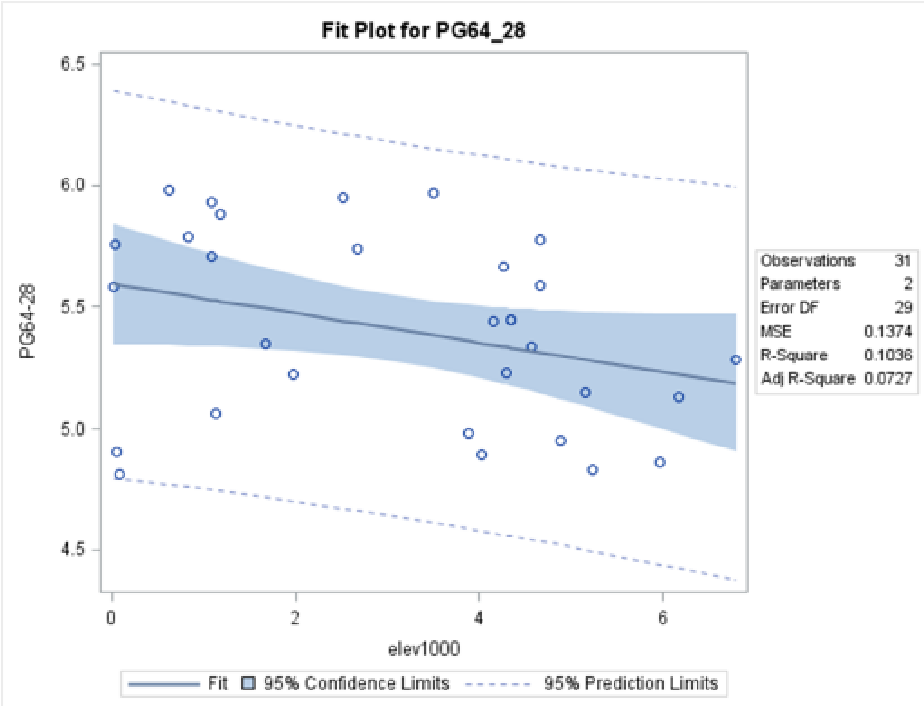

Figure 13: G* / sin δ Fit Plot PG64-28

Table 21: Test Results for G* / sin δ-PG64-28

PG64-28

Analysis of Variance					
Source	**DF**	**Sum of Squares**	**Mean Square**	**F Value**	**Pr > F**
Model	1	0.46075	0.46075	3.35	0.0774
Error	29	3.98454	0.13740		
Corrected Total	30	4.44528			

Parameter Estimates						
Variable	**Label**	**DF**	**Parameter Estimate**	**Standard Error**	**t Value**	**Pr > |t|**
Intercept	Intercept	**1**	5.59421	0.12151	46.04	<.0001
elev1000		**1**	-0.06019	0.03287	-1.83	0.0774

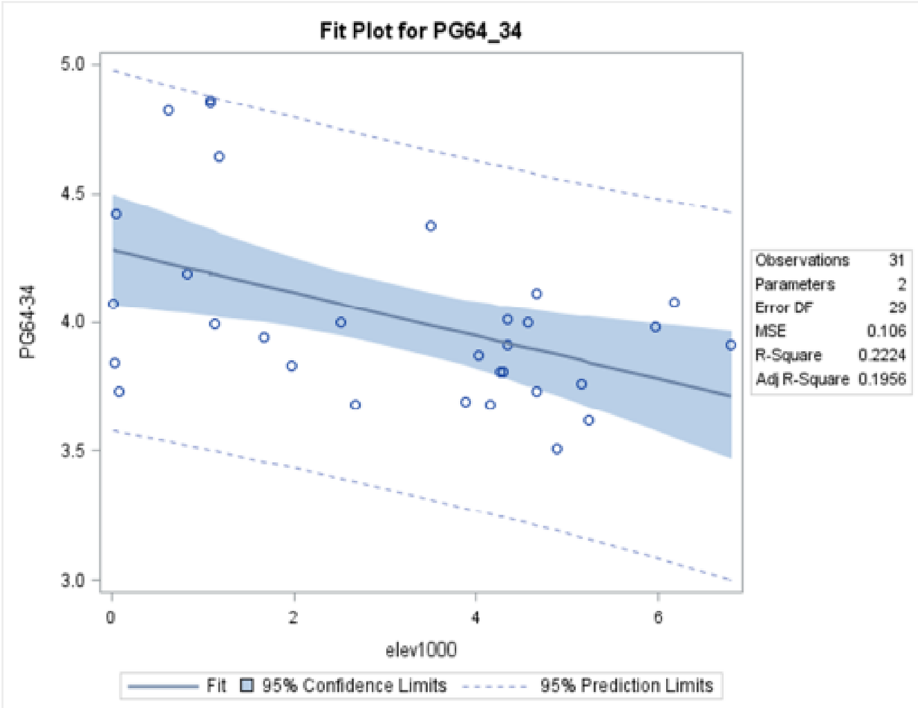

Figure 14: G* / sin δ Fit Plot PG64-34

Table 22: Test Results for G* / sin δ-PG64-34

PG64-34

Analysis of Variance					
Source	**DF**	**Sum of Squares**	**Mean Square**	**F Value**	**Pr > F**
Model	1	0.87915	0.87915	8.29	0.0074
Error	29	3.07429	0.10601		
Corrected Total	30	3.95344			

Parameter Estimates						
Variable	**Label**	**DF**	**Parameter Estimate**	**Standard Error**	**t Value**	**Pr > |t|**
Intercept	Intercept	**1**	4.28003	0.10673	40.10	<.0001
elev1000		**1**	-0.08314	0.02887	-2.88	0.0074

Table 23: Test Results for G* / sin δ-PG70-22

PG70-22

Analysis of Variance					
Source	**DF**	**Sum of Squares**	**Mean Square**	**F Value**	**Pr > F**
Model	1	1.18990	1.18990	1.66	0.2079
Error	29	20.79998	0.71724		
Corrected Total	30	21.98988			

Parameter Estimates						
Variable	**Label**	**DF**	**Parameter Estimate**	**Standard Error**	**t Value**	**Pr > |t|**
Intercept	Intercept	**1**	3.67236	0.27762	13.23	<.0001
elev1000		**1**	-0.09672	0.07509	-1.29	0.2079

Table 24: Test Results for G* / sin δ-PG70-28

PG70-28

Analysis of Variance					
Source	**DF**	**Sum of Squares**	**Mean Square**	**F Value**	**Pr > F**
Model	1	0.17750	0.17750	1.22	0.2781
Error	29	4.21259	0.14526		
Corrected Total	30	4.39008			

Parameter Estimates						
Variable	**Label**	**DF**	**Parameter Estimate**	**Standard Error**	**t Value**	**Pr > |t|**
Intercept	Intercept	**1**	4.01360	0.12494	32.12	<.0001
elev1000		**1**	-0.03736	0.03379	-1.11	0.2781

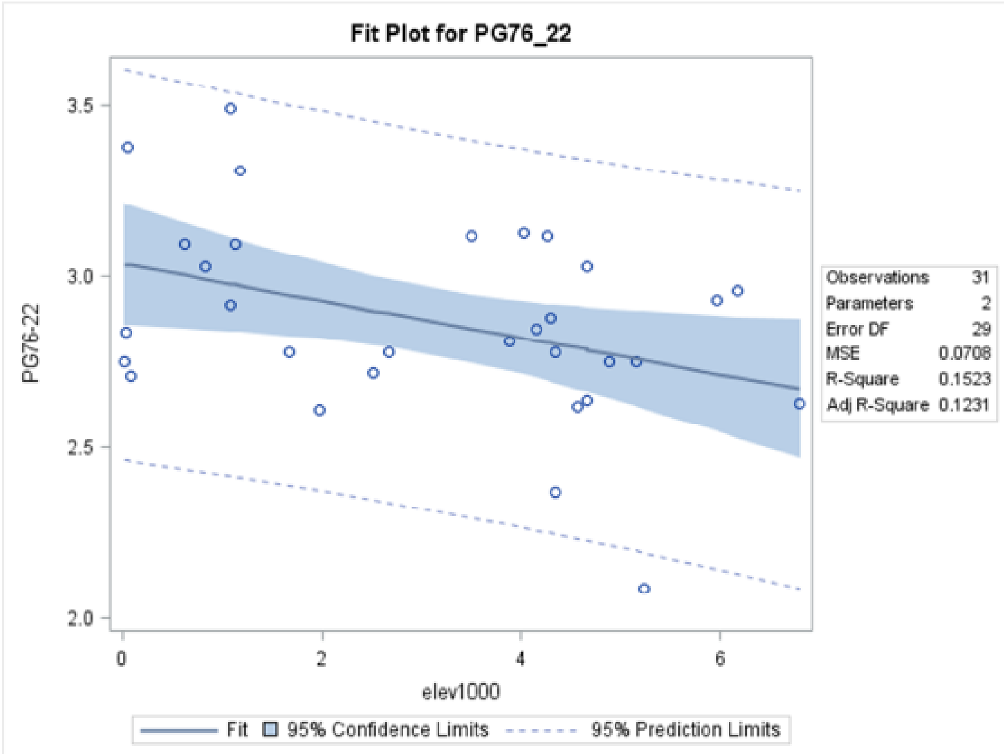

Figure 15: G* / sin δ Fit Plot PG76-22

Table 25: Test Results for G* / sin δ-PG76-22

PG76-22

Analysis of Variance					
Source	**DF**	**Sum of Squares**	**Mean Square**	**F Value**	**Pr > F**
Model	1	0.36886	0.36886	5.21	0.0300
Error	29	2.05263	0.07078		
Corrected Total	30	2.42150			

Parameter Estimates						
Variable	**Label**	**DF**	**Parameter Estimate**	**Standard Error**	**t Value**	**Pr > |t|**
Intercept	Intercept	**1**	3.03687	0.08721	34.82	<.0001
elev1000		**1**	-0.05385	0.02359	-2.28	0.0300

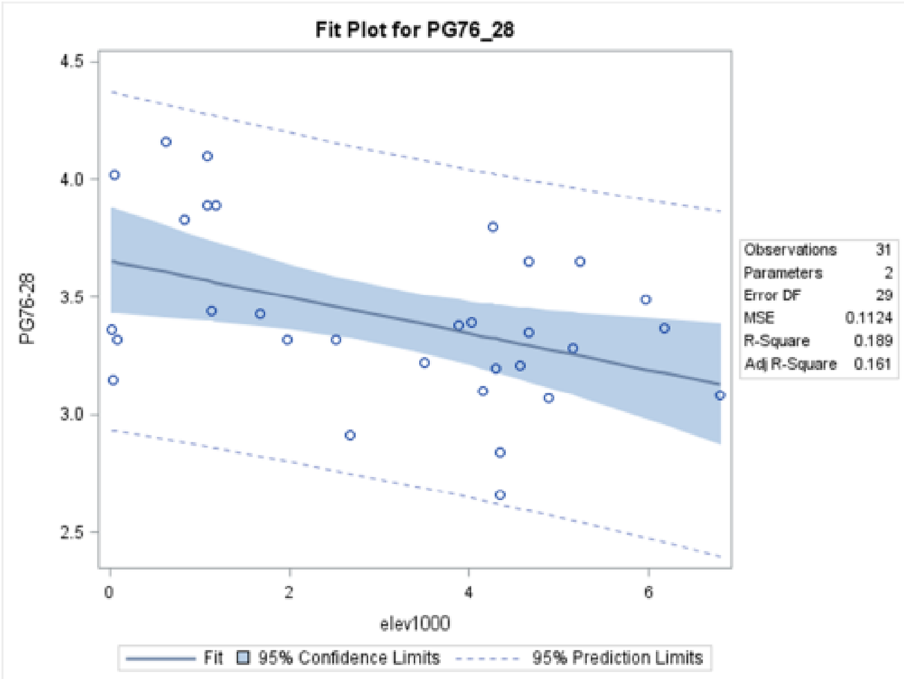

Figure 16: G* / sin δ Fit Plot PG76-28

Table 26: Test Results for G* / sin δ-PG76-28

PG76-28

Analysis of Variance

Source	DF	Sum of Squares	Mean Square	F Value	Pr > F
Model	1	0.75939	0.75939	6.76	0.0145
Error	29	3.25858	0.11236		
Corrected Total	30	4.01797			

Parameter Estimates

Variable	Label	DF	Parameter Estimate	Standard Error	t Value	Pr > |t|
Intercept	Intercept	**1**	3.65445	0.10988	33.26	<.0001
elev1000		**1**	-0.07727	0.02972	-2.60	0.0145

APPENDIX D: REGRESSION ANALYSIS OF THE DATA SET OF COMPLEX MODULUS (G*-6C)

Table 27: The Data Set of Complex Modulus (G*-6C)

Elevation Group(ft.)	Elevation (ft.)	LAB No.	PG 64-28	PG 64-34	PG 70-22	PG 70-28	PG 76-22	PG 76-28
0-500	21	39	5.09	5.25	6.39	4.94	3.8	4.63
	27	11	5.44	5.99	6.38	6.27	4.36	4.58
	37	52	5.36	5.73	4.82	6.09	4.27	4.9
	38	13	5.2	6.03	6.08	6.24	4.11	4.71
	47	69	4.41	5.73	7.62	4.26	4.24	5.95
	52	76	5.03	5.29	5.5	5.57		3.86
	78	31	4.46	4.99	5.55	4.88	3.77	4.62
	194	37	4.53	5.7	5.36	4.71		4.56
	196	73						
	355	55	4.87	5.92	5.47	5.91		5.3
	466	83						
	500	65	4.65				4.31	
501-1000	568	68						6.46
	615	64	5.38	5.35	6.29	5.93	4.25	5.64
	826	63	5.29	5.71	5.07	5.09	4.43	5.3
	879	71	5.79		7.37		4.47	5.33
1001-1500	1077	1	5.43	6.69	6.2	5.67	4.67	5.45
	1084	32	5.12	6.13	11.9	5.3	4.14	5.29
	1095	81						
	1127	56	4.64	5.33	5.72	4.58	4.36	4.81
	1135	23	4.2		11.7		4.17	7.15
	1185	24	5.38	5.96	6.15	5.24	4.51	5.48
1501-2000	1678	26	4.91	5.34	6.64	5.07	4.01	4.87
	1974	59	4.94	4.8	4.62	5.61		4.76
2001-2500	2111	75		5.12				4.91
	2244	3	5.51		3.93		4.13	3.86
	2333	66		4.7	6.03	5.41	3.72	3.7
	2458	77			5.78	5.49		3.89
2501-3000	2523	17	5.47	5.17	5.76	5.4	4.08	4.39
	2535	78						
	2583	74						
	2673	18	5.16	5.5	3.44	5.53	4.17	4.53
	2902	4						

Table 27: The Data Set of Complex Modulus (G*-6C)-continued

3001-3500	3103	14	5.24		5.58	5.4	4.1	5.36
	3187	50						
	3258	80						
	3349	22						
	3380	60						
3501-4000	3507	42	4.97		5.94	5.01	4.26	4.77
	3632	79						
	3879	49	4.58	5.18	6.27	4.53	4.25	5.17
4001-4500	4028	21	4.64	5.55	6.47	4.77	4.31	4.95
	4157	35	4.99	5.44	5.1	4.75	4.01	4.48
	4267	19	5.11	5.29	7.1	7.86	4.27	4.94
	4294	2	4.78	5.3	6.56	5.37	4.41	4.57
	4342	38	5.01	5.56	4.25	4.67	3.4	4.14
	4342	30	4.98	5.43	5.8	4.23	3.94	4.63
4501-5000	4568	45	4.91	5.62	5.14	5.25	4.13	4.73
	4657	5	5.04	5.38	4.81	4.89	3.94	4.74
	4665	46	5.33	5.3	4.87	4.48	4.4	4.89
	4872	82						
	4882	10	4.54	4.81	4.28	4.48	3.77	5.19
	4987	57	4.95					
5001-5500	5153	8	4.73	4.96	5.93	4.79	4.09	4.63
	5240	72	4.44	4.92	5.76	4.53	3.75	5.3
	5445	6	4.67	5.3	5.3	5.58		4.68
5501-6000	5555	16						
	5613	15					4.38	
	5971	47	4.47	5.24	6.15	5.02	4.05	5.02
6001-6500	6178	40	4.7	5.31	5.33	4.82	4.13	4.83
6501-7000	6588	33	5.6	4.85	7.22	3.47	3.82	5.02
	6798	41	4.99	5.38	4.68	5.57	3.51	4.24
	6901	25			5.12		3.83	

G* -6C Regression Analysis

Table 28: Test Results for Complex Modulus (-6C)-PG64-28

PG64-28

Analysis of Variance					
Source	**DF**	**Sum of Squares**	**Mean Square**	**F Value**	**Pr > F**
Model	1	0.24685	0.24685	2.10	0.1579
Error	30	3.52984	0.11766		
Corrected Total	31	3.77669			

Parameter Estimates						
Variable	**Label**	**DF**	**Parameter Estimate**	**Standard Error**	**t Value**	**Pr > |t|**
Intercept	Intercept	**1**	5.10728	0.10289	49.64	<.0001
elev1000		**1**	-0.03970	0.02741	-1.45	0.1579

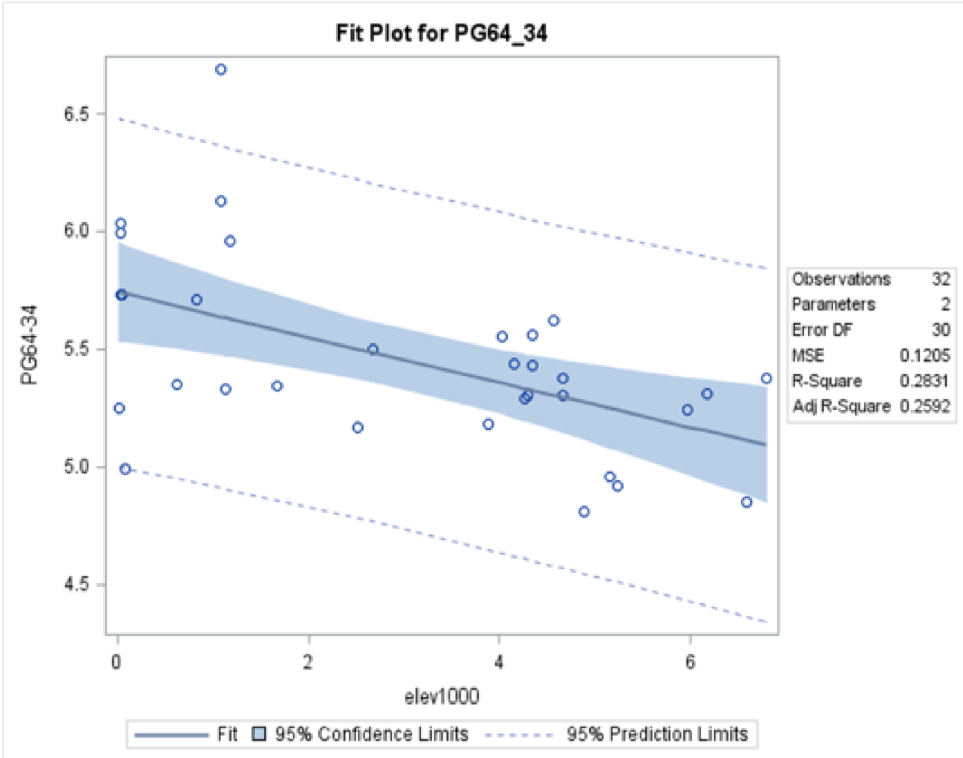

Figure 17: Complex Modulus (G*-6C) Fit Plot PG64-34

Table 29: Test Results for Complex Modulus (-6C)-PG64-34

PG64-34

Analysis of Variance					
Source	**DF**	**Sum of Squares**	**Mean Square**	**F Value**	**Pr > F**
Model	1	1.42688	1.42688	11.85	0.0017
Error	30	3.61370	0.12046		
Corrected Total	31	5.04059			

Parameter Estimates						
Variable	**Label**	**DF**	**Parameter Estimate**	**Standard Error**	**t Value**	**Pr > |t|**
Intercept	Intercept	**1**	5.74010	0.10411	55.14	<.0001
elev1000		**1**	-0.09545	0.02773	-3.44	0.0017

Table 30: Test Results for Complex Modulus (-6C)-PG70-22

PG70-22

Analysis of Variance					
Source	**DF**	**Sum of Squares**	**Mean Square**	**F Value**	**Pr > F**
Model	1	3.89391	3.89391	1.97	0.1706
Error	30	59.27356	1.97579		
Corrected Total	31	63.16747			

Parameter Estimates						
Variable	**Label**	**DF**	**Parameter Estimate**	**Standard Error**	**t Value**	**Pr > |t|**
Intercept	Intercept	**1**	6.40727	0.42164	15.20	<.0001
elev1000		**1**	-0.15769	0.11232	-1.40	0.1706

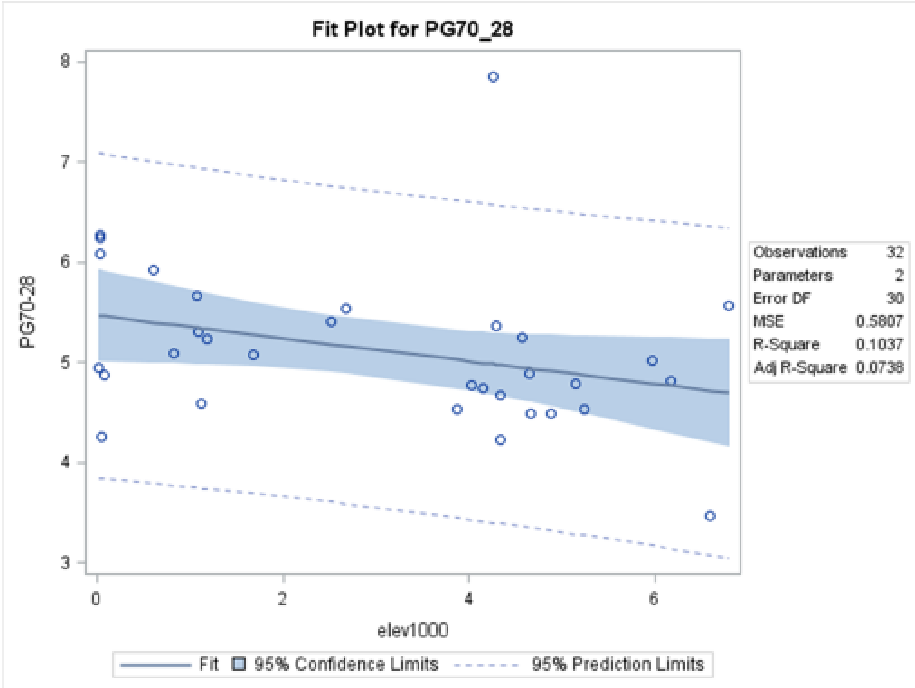

Figure 18: Complex Modulus (G*-6C) Fit Plot PG70-28

Table 31: Test Results for Complex Modulus (-6C)-PG70-28

PG70-28

Analysis of Variance					
Source	**DF**	**Sum of Squares**	**Mean Square**	**F Value**	**Pr > F**
Model	1	2.01535	2.01535	3.47	0.0723
Error	30	17.42163	0.58072		
Corrected Total	31	19.43697			

Parameter Estimates						
Variable	**Label**	**DF**	**Parameter Estimate**	**Standard Error**	**t Value**	**Pr > |t|**
Intercept	Intercept	**1**	5.46809	0.22859	23.92	<.0001
elev1000		**1**	-0.11344	0.06090	-1.86	0.0723

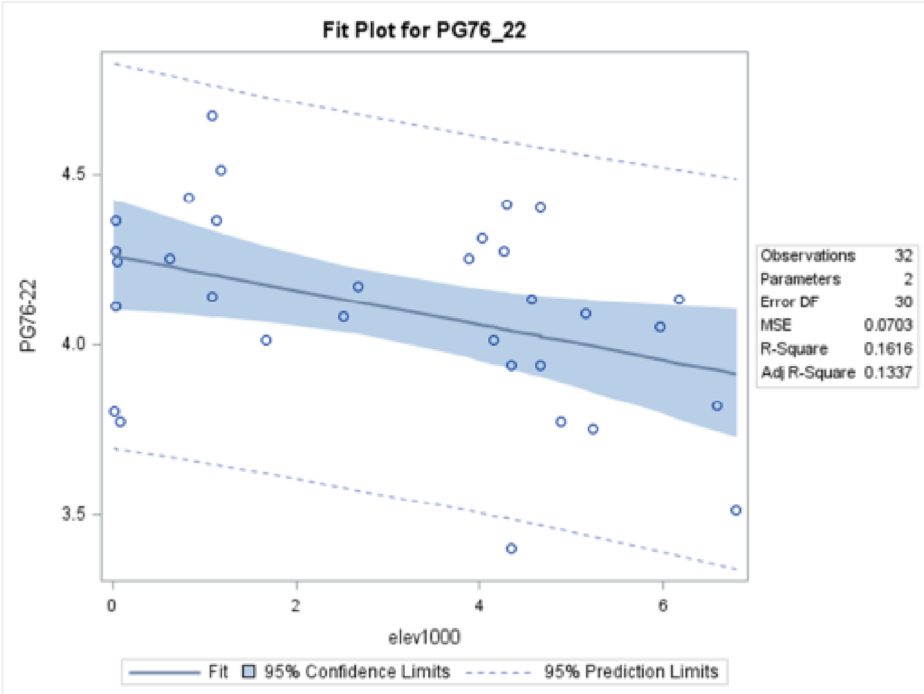

Figure 19: Complex Modulus (G*-6C) Fit Plot PG76-22

Table 32: Test Results for Complex Modulus (-6C)-PG76-22

PG76-22

Analysis of Variance					
Source	**DF**	**Sum of Squares**	**Mean Square**	**F Value**	**Pr > F**
Model	1	0.40642	0.40642	5.78	0.0226
Error	30	2.10818	0.07027		
Corrected Total	31	2.51460			

Parameter Estimates						
Variable	**Label**	**DF**	**Parameter Estimate**	**Standard Error**	**t Value**	**Pr > |t|**
Intercept	Intercept	**1**	4.25918	0.07952	53.56	<.0001
elev1000		**1**	-0.05094	0.02118	-2.40	0.0226

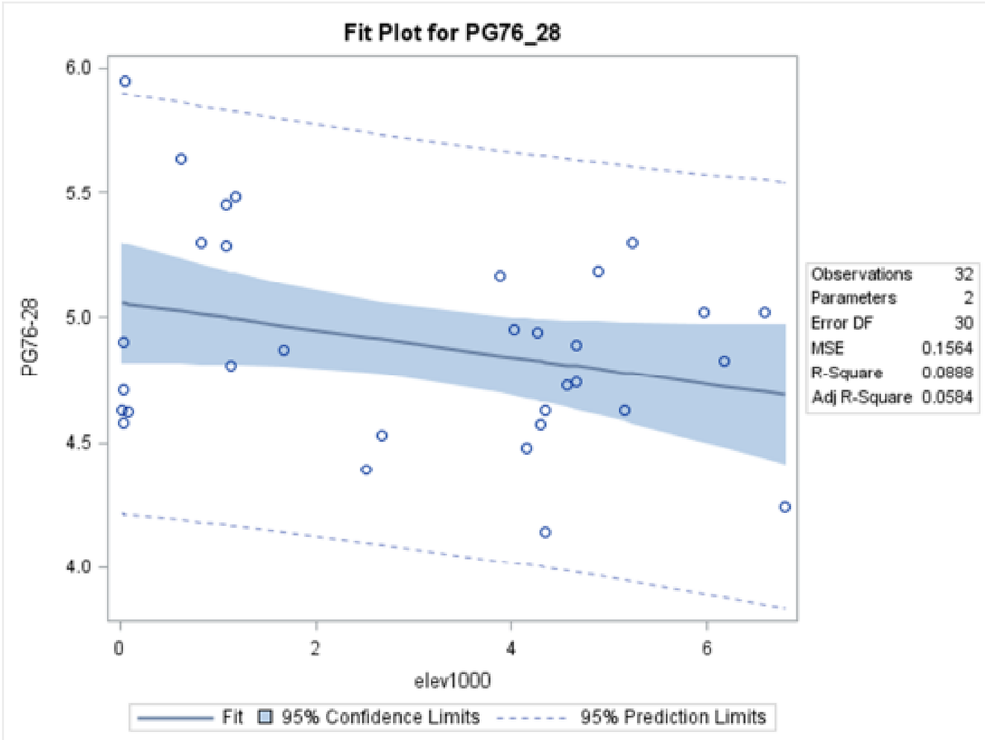

Figure 20: Complex Modulus (G*-6C) Fit Plot PG76-28

Table 33: Test Results for Complex Modulus (-6C)-PG76-28

PG76-28

Analysis of Variance

Source	DF	Sum of Squares	Mean Square	F Value	Pr > F
Model	1	0.45740	0.45740	2.92	0.0976
Error	30	4.69219	0.15641		
Corrected Total	31	5.14959			

Parameter Estimates

Variable	Label	DF	Parameter Estimate	Standard Error	t Value	Pr > |t|
Intercept	Intercept	1	5.05827	0.11863	42.64	<.0001
elev1000		1	-0.05404	0.03160	-1.71	0.0976

APPENDIX E: ANALYSIS OF THE DATA SET FOR PHASE ANGLE (Δ–6C)

Table 34: The Data Set of Phase Angle (δ–6C)

Elevation Group(ft.)	Elevation (ft.)	LAB No.	PG 64-28	PG 64-34	PG 70-22	PG 70-28	PG 76-22	PG 76-28
0-500	21	39	66.27	50.7	65.65	63.6	59.5	56.98
	27	11	66	54.55	66.83	62.1	59.5	56.22
	37	52	64.15	50.5	69.88	62.1	59.55	56.68
	38	13	64.55	50.3	67.73	62.7	59.8	57.7
	47	69	64.2	55.7	66.97	64.4	59.9	55.1
	52	76	71.1	58	70.9	62.7		60.7
	78	31	68.35	55.2	67.75	63.7	60	56.8
	194	37	67.55	54.05	67.65	63.55		56.93
	196	73						
	355	55	63.95	50.1	66.57	61.9		55.93
	466	83						
	500	65	63.4				60.2	
501-1000	568	68						55.8
	615	64	63.95	51	63.67	62.2	59.1	54.75
	826	63	66.2	54.5	69.35	63.6	59.4	55.95
	879	71	63.45		63.53		58.9	55
1001-1500	1077	1	66.23	54.25	67.48	63.15	58.85	55.93
	1084	32	63.75	51.3	61	63	48.95	54.8
	1095	81						
	1127	56	66.77	55.15	67.48	64.25	59.85	56.68
	1135	23	63.5		60		59.9	54.5
	1185	24	66.3	51	66.95	63.5	58.9	55.6
1501-2000	1678	26	66.93	54.85	65.08	63.25	59.85	56.63
	1974	59	71.3	51.2	70.55	62.5		57.35
2001-2500	2111	75		51.2				55.5
	2244	3	65		59.4		59.2	55.7
	2333	66		50.7	65.9	63.8	59.95	55.9
	2458	77				62.1		60.1
2501-3000	2523	17	67.6	56.5	67.83	63	60.75	56.7
	2535	78						
	2583	74						
	2673	18	64.05	51.1	70.1	62.7	59.45	56.78
	2902	4						

Table 34: The Data Set of Phase Angle (δ–6C)-continued

3001-3500	3103	14	64.55		65.5	62.9	59.4	55.6
	3187	50						
	3258	80						
	3349	22						
	3380	60						
3501-4000	3507	42	66.67		65.8	63.5	59.1	57.03
	3632	79						
	3879	49	67.15	50.6	69.8	63.4	60.1	56.03
4001-4500	4028	21	71.7	55.3	65.6	64.05	59.85	56.95
	4157	35	66.6	55.4	71.2	64.05	59.75	57.43
	4267	19	64.2	55.8	60.9	62.4	58.9	57.87
	4294	2	66.9	50.6	64.27	62.9	59.7	57.17
	4342	38	66.9	54.9	70.78	64	59.95	57.4
	4342	30	66.43	54.55	66.28	65.2	59.9	57.63
4501-5000	4568	45	66.67	54.7	72.63	63.75	60.05	57.35
	4657	5	64.3	51.6	65.1	63.85	60.3	57.3
	4665	46	67.4	54.9	66.43	63.45	59.4	55.48
	4872	82						
	4882	10	66.83	56.4	64.45	63.9	59.8	56.73
	4987	57	65.3					
5001-5500	5153	8	66.9	55	65.85	63.7	59.95	57.05
	5240	72	67.45	51.6	70.6	64.35	60.7	56.25
	5445	6	67.2	52.2	68.4	62.6		57.37
5501-6000	5555	16						
	5613	15					58.5	
	5971	47	67.2	51.6	67.1	63.8	59.75	56.73
6001-6500	6178	40	66.63	54.95	68.38	63.85	59.7	56.63
6501-7000	6588	33	65.6	55.3	70.8	65.5	59.8	55.93
	6798	41	70.9	55.55	67.6	62.8	59.95	56.8
	6901	25					59.7	

Delta -6C Regression Analysis

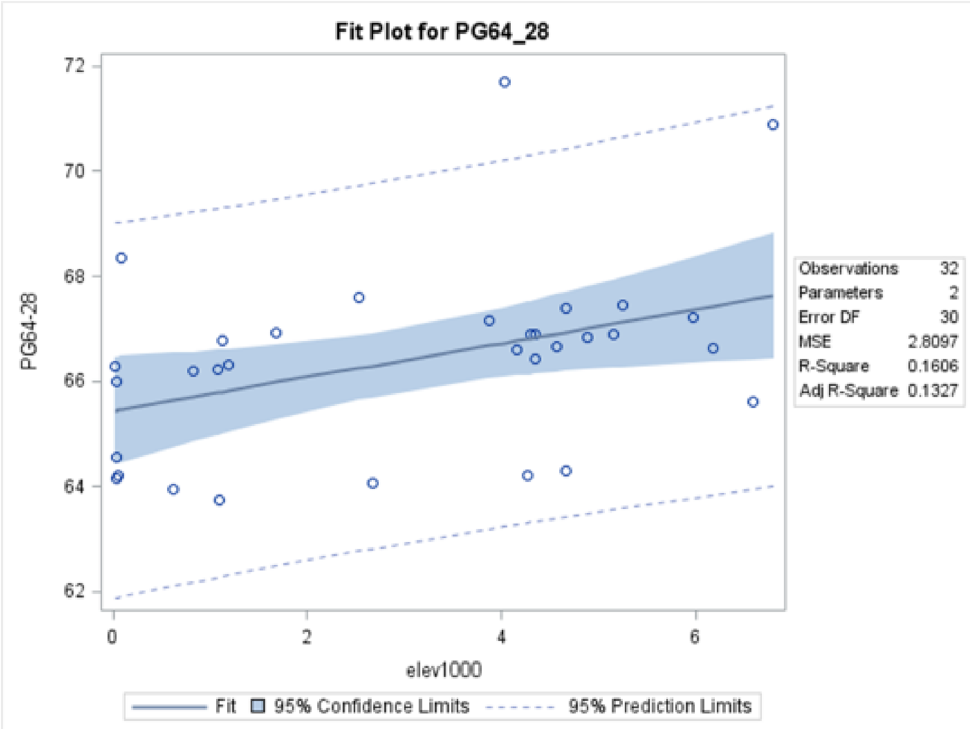

Figure 21: Phase Angle (δ-6C) Fit Plot PG76-28

Table 35: Test Results for Phase Angle (-6C)-PG64-28

PG64-28

Analysis of Variance					
Source	**DF**	**Sum of Squares**	**Mean Square**	**F Value**	**Pr > F**
Model	1	16.13284	16.13284	5.74	0.0230
Error	30	84.29024	2.80967		
Corrected Total	31	100.42309			

Parameter Estimates						
Variable	**Label**	**DF**	**Parameter Estimate**	**Standard Error**	**t Value**	**Pr > |t|**
Intercept	Intercept	**1**	65.43476	0.50280	130.14	<.0001

Parameter Estimates						
Variable	**Label**	**DF**	**Parameter Estimate**	**Standard Error**	**t Value**	**Pr > |t|**
elev1000		**1**	0.32096	0.13394	2.40	0.0230

Table 36: Test Results for Phase Angle (-6C)-PG64-34

PG64-34

Analysis of Variance					
Source	**DF**	**Sum of Squares**	**Mean Square**	**F Value**	**Pr > F**
Model	1	10.34147	10.34147	2.39	0.1327
Error	30	129.88533	4.32951		
Corrected Total	31	140.22680			

Parameter Estimates						
Variable	**Label**	**DF**	**Parameter Estimate**	**Standard Error**	**t Value**	**Pr > |t|**
Intercept	Intercept	**1**	52.82537	0.62415	84.64	<.0001
elev1000		**1**	0.25697	0.16627	1.55	0.1327

Table 37: Test Results for Phase Angle (-6C)-PG70-22

PG70-22

Analysis of Variance					
Source	**DF**	**Sum of Squares**	**Mean Square**	**F Value**	**Pr > F**
Model	1	5.76664	5.76664	0.75	0.3935
Error	30	230.80916	7.69364		
Corrected Total	31	236.57580			

Parameter Estimates						
Variable	**Label**	**DF**	**Parameter Estimate**	**Standard Error**	**t Value**	**Pr > |t|**
Intercept	Intercept	**1**	66.65305	0.83202	80.11	<.0001
elev1000		**1**	0.19189	0.22165	0.87	0.3935

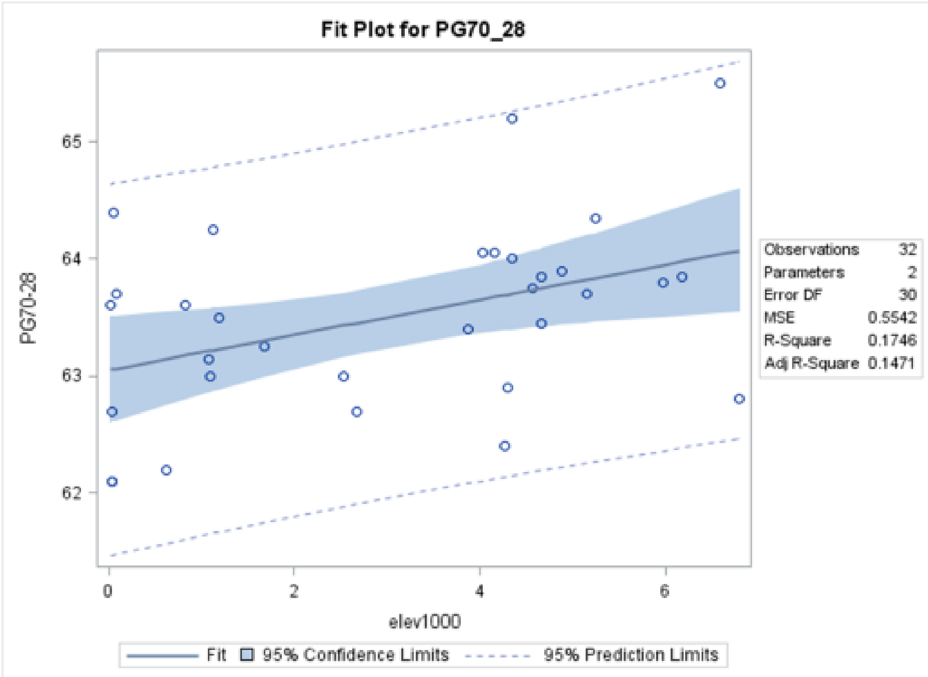

Figure 22: Phase Angle (δ-6C) Fit Plot PG70-28

Table 38: Test Results for Phase Angle (-6C)-PG70-28

PG70-28

Analysis of Variance					
Source	**DF**	**Sum of Squares**	**Mean Square**	**F Value**	**Pr > F**
Model	1	3.51642	3.51642	6.34	0.0173
Error	30	16.62733	0.55424		
Corrected Total	31	20.14375			

Parameter Estimates						
Variable	**Label**	**DF**	**Parameter Estimate**	**Standard Error**	**t Value**	**Pr > |t|**
Intercept	Intercept	**1**	63.05182	0.22332	282.34	<.0001
elev1000		**1**	0.14985	0.05949	2.52	0.0173

Table 39: Test Results for Phase Angle (-6C)-PG76-22

PG76-22

Analysis of Variance

Source	DF	Sum of Squares	Mean Square	F Value	Pr > F
Model	1	6.00686	6.00686	1.60	0.2157
Error	30	112.64783	3.75493		
Corrected Total	31	118.65469			

Parameter Estimates

Variable	Label	DF	Parameter Estimate	Standard Error	t Value	Pr > |t|
Intercept	Intercept	**1**	58.80918	0.58126	101.18	<.0001
elev1000		**1**	0.19585	0.15485	1.26	0.2157

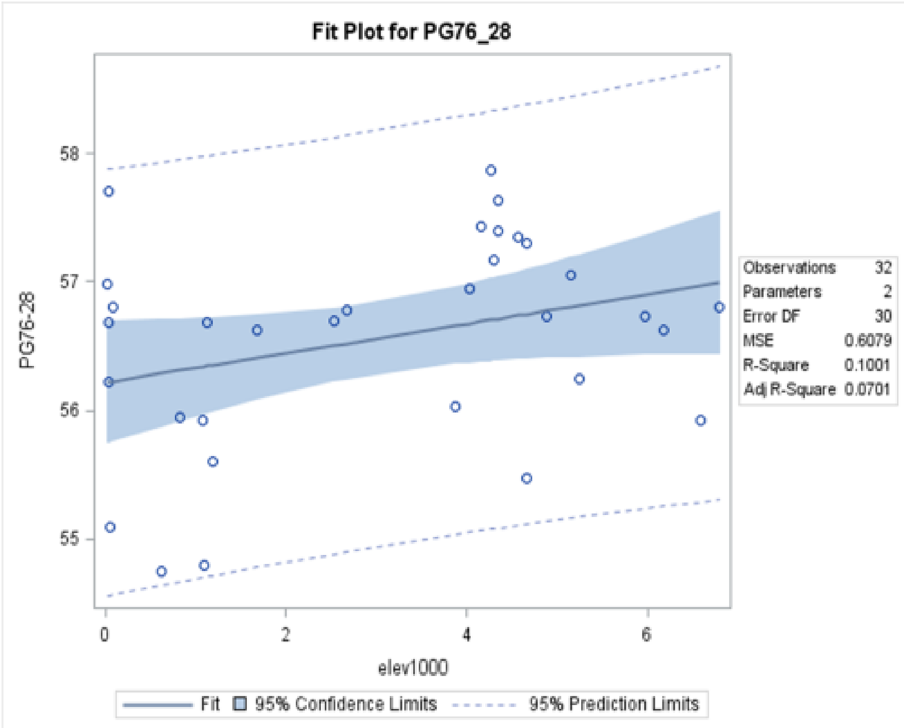

Figure 23: Phase Angle (δ-6C) Fit Plot PG76-28

Table 40: Test Results for Phase Angle (-6C)-PG76-28

PG76-28

Analysis of Variance					
Source	**DF**	**Sum of Squares**	**Mean Square**	**F Value**	**Pr > F**
Model	1	2.02927	2.02927	3.34	0.0777
Error	30	18.23726	0.60791		
Corrected Total	31	20.26652			

Parameter Estimates						
Variable	**Label**	**DF**	**Parameter Estimate**	**Standard Error**	**t Value**	**Pr > |t|**
Intercept	Intercept	**1**	56.21822	0.23388	240.38	<.0001
elev1000		**1**	0.11383	0.06230	1.83	0.0777

APPENDIX F: ANALYSIS OF THE DATA SET FOR G*/SIN – 6C

Table 41: The Data for G*/sin – 6C

Elevation Group(ft.)	Elevation (ft.)	LAB No.	PG 64-28	PG 64-34	PG 70-22	PG 70-28	PG 76-22	PG 76-28
0-500	21	39	5.58	6.79	5.42	5.52	4.41	5.52
	27	11	5.97	7.36	6.96	7.1	5.05	5.51
	37	52	5.95	7.42	5.18	6.89	4.96	5.88
	38	13	5.76	7.84	6.56	7.02	4.75	5.59
	47	69	4.9	6.9	8.49	4.73	4.9	7.27
	52	76	5.32	6.79	5.83	6.27		4.42
	78	31	4.81	6.1	5.99	5.46	4.35	5.54
	194	37	4.9	7.05	5.79	5.27		5.45
	196	73						
	355	55	5.42	7.71	5.96	6.7		6.42
	466	83						
	500	65	5.2				4.97	
501-1000	568	68						7.81
	615	64	5.98	6.91	7.09	6.7	4.95	6.92
	826	63	5.79	7.07	5.44	5.7	5.15	6.43
	879	71	6.46		8.34		5.22	6.51
1001-1500	1077	1	5.93	8.3	6.7	6.36	5.45	6.62
	1084	32	5.71	7.86	13.6	5.97	4.44	6.49
	1095	81						
	1127	56	5.06	6.51	6.21	5.1	5.04	5.77
	1135	23	4.7		13.5		4.82	8.78
	1185	24	5.88	7.67	6.69	5.85	5.27	6.67
1501-2000	1678	26	5.35	6.56	7.46	5.68	4.65	5.87
	1974	59	5.22	6.15	4.94	6.32		5.66
2001-2500	2111	75		6.52				5.96
	2244	3	6.08		4.57		4.81	4.67
	2333	66		6.07	6.7	6.03	4.29	4.47
	2458	77			6.29	6.21		4.49
2501-3000	2523	17	5.95	6.22	6.24	6.06	4.67	5.27
	2535	78						
	2583	74						
	2673	18	5.74	7.07	3.74	6.22	4.85	5.42
	2902	4						

Table 41: The Data for G*/sin–6C-continued

3001-3500	3103	14	5.8		6.09	6.08	4.76	6.48
	3187	50						
	3258	80						
	3349	22						
	3380	60						
3501-4000	3507	42	5.42		5.13	5.61	4.97	5.69
	3632	79						
	3879	49	4.98	6.7	6.69	5.08	4.91	6.29
4001-4500	4028	21	4.89	6.78	7.22	5.31	4.98	5.94
	4157	35	5.44	6.64	5.4	5.29	4.64	5.34
	4267	19	5.67	6.42	8.12	8.87	5.01	5.85
	4294	2	5.23	6.87	7.36	6.04	5.13	5.46
	4342	38	5.45	6.8	3.79	5.21	3.93	4.92
	4342	30	5.45	6.7	6.44	4.66	4.56	6.06
4501-5000	4568	45	5.34	6.93	5.39	5.41	4.77	5.62
	4657	5	5.59	6.87	5.29	5.46	4.55	5.65
	4665	46	5.78	6.5	5.34	5.01	5.11	6.01
	4872	82						
	4882	10	4.95	5.81	4.75	4.49	4.36	6.26
	4987	57	5.45					
5001-5500	5153	8	5.15	6.09	6.57	5.35	4.68	5.53
	5240	72	4.83	6.28	5.94	5.03	4.3	6.38
	5445	6	5.08	6.7	5.69	6.28		5.58
5501-6000	5555	16						
	5613	15					5.14	
	5971	47	4.86	6.68	6.69	5.61	4.69	6.04
6001-6500	6178	40	5.13	6.52	5.73	5.38	4.78	5.8
6501-7000	6588	33	6.15	5.94		3.81	4.41	6.06
	6798	41	5.28	6.54	5.06	6.26	4.05	5.09
	6901	25			5.46		4.43	

G*/sin δ-6C Regression Analysis

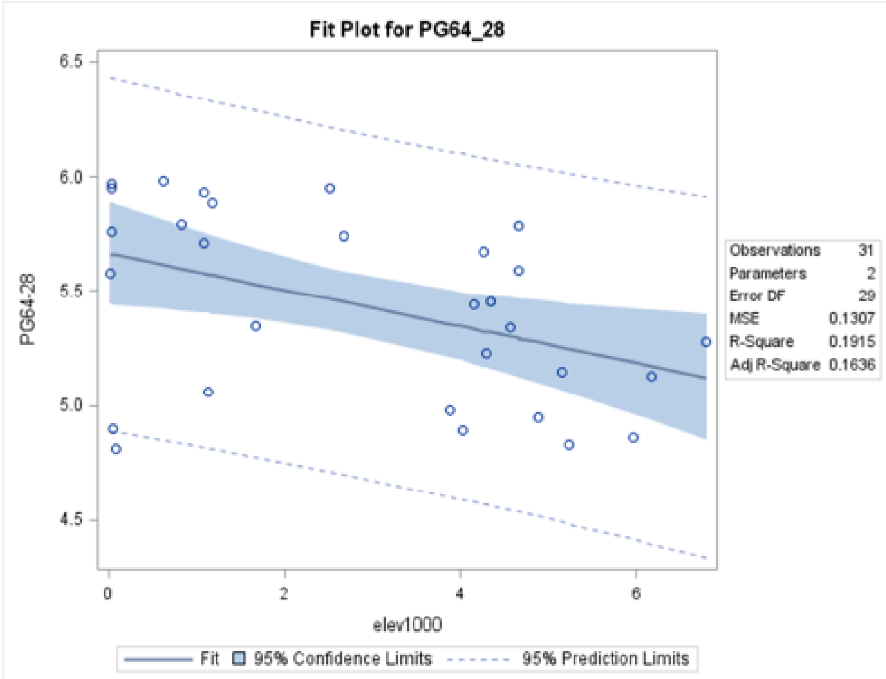

Figure 24: G*/sin δ (-6C) Fit Plot PG64-28

Table 42: Test Results for G*/sin δ (-6C)-PG64-28

PG64-28

Analysis of Variance					
Source	**DF**	**Sum of Squares**	**Mean Square**	**F Value**	**Pr > F**
Model	1	0.89730	0.89730	6.87	0.0138
Error	29	3.78912	0.13066		
Corrected Total	30	4.68642			

Parameter Estimates						
Variable	**Label**	**DF**	**Parameter Estimate**	**Standard Error**	**t Value**	**Pr > |t|**
Intercept	Intercept	**1**	5.66231	0.10938	51.77	<.0001
elev1000		**1**	-0.07906	0.03017	-2.62	0.0138

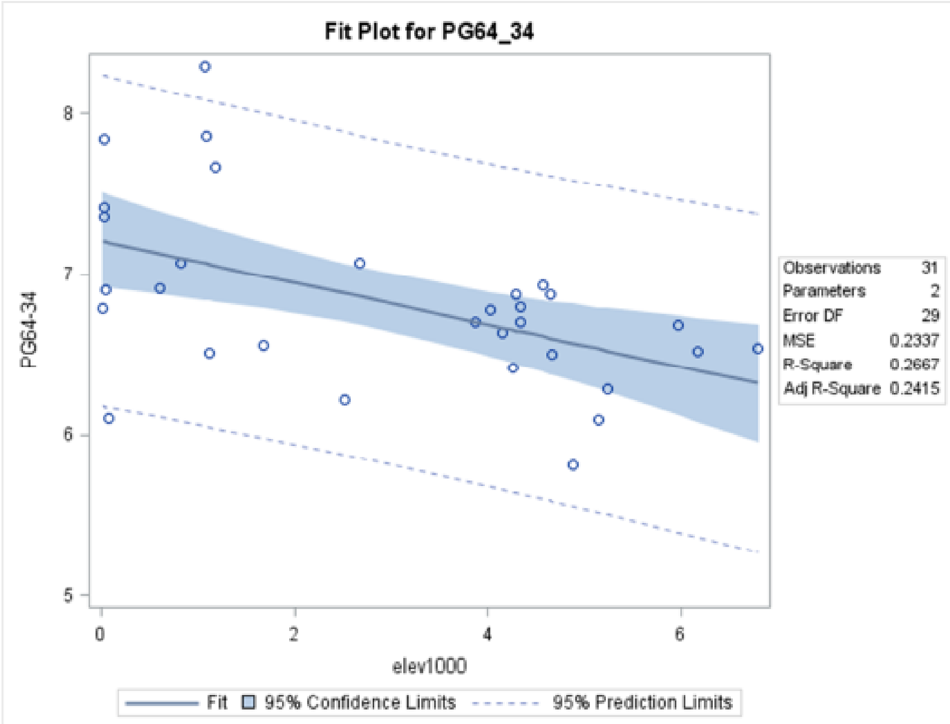

Figure 25: G*/sin δ (-6C) Fit Plot PG64-34

Table 43: Test Results for G*/sin δ(-6C)-PG64-34

PG64-34

Analysis of Variance

Source	DF	Sum of Squares	Mean Square	F Value	Pr > F
Model	1	2.46509	2.46509	10.55	0.0029
Error	29	6.77649	0.23367		
Corrected Total	30	9.24159			

Parameter Estimates

Variable	Label	DF	Parameter Estimate	Standard Error	t Value	Pr > |t|
Intercept	Intercept	**1**	7.21173	0.14628	49.30	<.0001
elev1000		**1**	-0.13104	0.04035	-3.25	0.0029

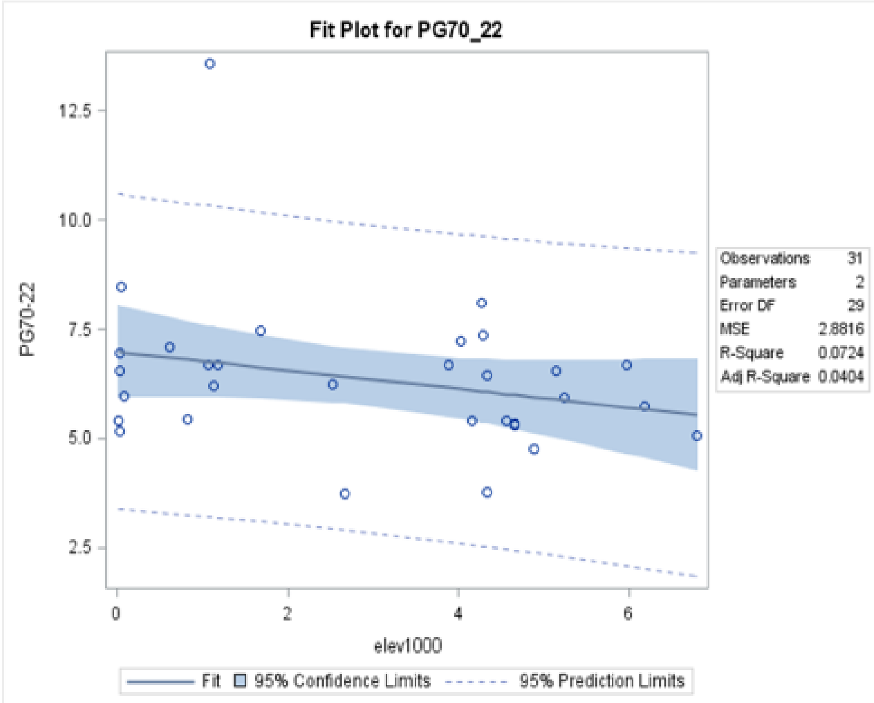

Figure 26: G*/sin δ (-6C) Fit Plot PG70-22

Table 44: Test Results for G*/sin δ (-6C)-PG70-22

PG70-22

Analysis of Variance					
Source	**DF**	**Sum of Squares**	**Mean Square**	**F Value**	**Pr > F**
Model	1	6.52494	6.52494	2.26	0.1432
Error	29	83.56625	2.88159		
Corrected Total	30	90.09119			

Parameter Estimates						
Variable	**Label**	**DF**	**Parameter Estimate**	**Standard Error**	**t Value**	**Pr > |t|**
Intercept	Intercept	**1**	6.99468	0.51368	13.62	<.0001
elev1000		**1**	-0.21320	0.14168	-1.50	0.1432

Table 45: Test Results for G*/sin δ (-6C)-PG70-28

PG70-28

Analysis of Variance					
Source	**DF**	**Sum of Squares**	**Mean Square**	**F Value**	**Pr > F**
Model	1	1.70937	1.70937	2.27	0.1429
Error	29	21.85465	0.75361		
Corrected Total	30	23.56402			

Parameter Estimates						
Variable	**Label**	**DF**	**Parameter Estimate**	**Standard Error**	**t Value**	**Pr > |t|**
Intercept	Intercept	**1**	6.08680	0.26269	23.17	<.0001
elev1000		**1**	-0.10912	0.07245	-1.51	0.1429

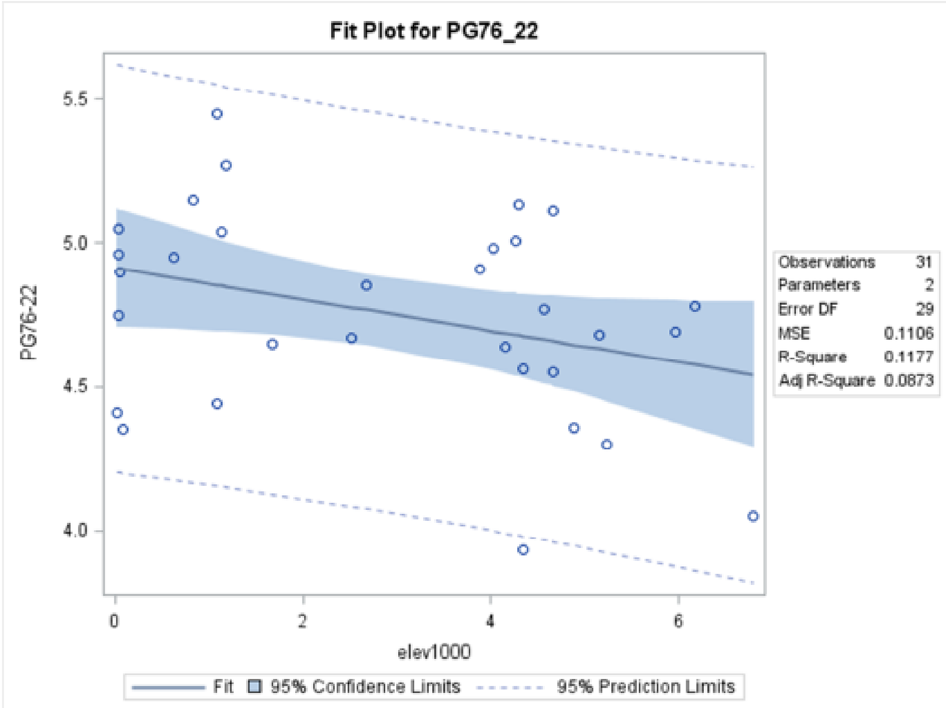

Figure 27: G*/sin δ (-6C) Fit Plot PG76-22

Table 46: Test Results for G*/sin δ (-6C)-PG76-22

PG76-22

Analysis of Variance					
Source	**DF**	**Sum of Squares**	**Mean Square**	**F Value**	**Pr > F**
Model	1	0.42766	0.42766	3.87	0.0589
Error	29	3.20638	0.11056		
Corrected Total	30	3.63404			

Parameter Estimates						
Variable	**Label**	**DF**	**Parameter Estimate**	**Standard Error**	**t Value**	**Pr > |t|**
Intercept	Intercept	**1**	4.91217	0.10062	48.82	<.0001
elev1000		**1**	-0.05458	0.02775	-1.97	0.0589

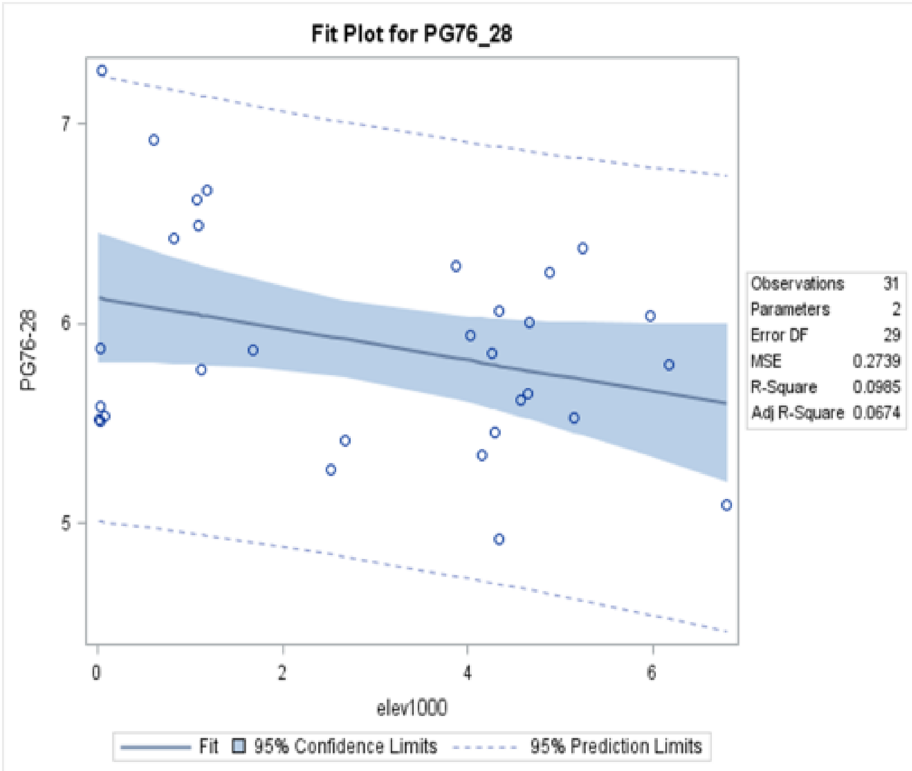

Figure 28: G*/sin δ (-6C) Fit Plot PG76-28

Table 47: Test Results for G*/sin δ (-6C)-PG76-28

PG76-28

Analysis of Variance					
Source	**DF**	**Sum of Squares**	**Mean Square**	**F Value**	**Pr > F**
Model	1	0.86788	0.86788	3.17	0.0855
Error	29	7.94203	0.27386		
Corrected Total	30	8.80991			

Parameter Estimates						
Variable	**Label**	**DF**	**Parameter Estimate**	**Standard Error**	**t Value**	**Pr > |t|**
Intercept	Intercept	**1**	6.13043	0.15836	38.71	<.0001
elev1000		**1**	-0.07775	0.04368	-1.78	0.0855

APPENDIX G: REGRESSION ANALYSIS FOR DATA SET OF DUCTILITY

Table 48: The Data Set for Ductility

Elevation Group(ft.)	Elevation (ft.)	LAB No.	PG 64-28	PG 64-34	PG 70-22	PG 70-28	PG 76-22	PG 76-28
0-500	21	39	24.27	31.3	10.83	16	22.5	12.5
	27	11						
	37	52						
	38	13						
	47	69	52.8	23.25	4.3	23	21.3	13.33
	52	76	15.5	28.5	5.75	16.5		17
	78	31	21.2	21.2	11.1	17.3	19.3	13.25
	194	37	16.8	25.65	26.37	23.1		16.1
	196	73						
	355	55	36.65		38			13.3
	466	83						
	500	65						
501-1000	568	68						
	615	64	22.17	28	15.75	11		2
	826	63	24.8	21.15	9.83	15.1	20.8	12.1
	879	71						
1001-1500	1077	1	24	19.25	12.38	16.85	19.3	11.57
	1084	32	33.5		4	21	10	16.25
	1095	81						
	1127	56	37.4	21.1	16.3	19.15	30	16.23
	1135	23						
	1185	24	25	22.2	0.5	13.75		11.83
1501-2000	1823	26	29.5	21.15	11.45	15.5	22	12.58
	1974	59	23.5	34	31		21	16
2001-2500	2111	75						
	2244	3	32.2		32.6			15
	2333	66			9.63			
	2458	77			5	36		29
2501-3000	2523	17	18	20.55	9.48	15	18	11.67
	2535	78						
	2583	74						
	2673	18						
	2902	4						

Table 48: The Data Set for Ductility-continued

3001-3500	3103	14							
	3187	50							
	3258	80							
	3349	22							
	3380	60							
3501-4000	3507	42							
	3632	79							
	3879	49							
4001-4500	4028	21		11.5	34				
	4157	35	25.67	24	6.95	19.5	19	18.67	
	4267	19	41.15	26	22.5			16	
	4294	2			7				
	4342	38	30.83	33.5	14	19	14	12.5	
	4342	30	28.73	26.4	14.25	23.4	39	14.57	
4501-5000	4568	45	30.33	20.25	1.47	17.25	17	12.67	
	4657	5	33.5	30	18	19	15	14	
	4665	46	33.3	24.5	13.73	16.55	23	16.67	
	4872	82							
	4882	10							
	4987	57							
5001-5500	5153	8	31.83	21.5	11.33	13	20.3	12.33	
	5240	72							
	5445	6	31.27	29	12.53	16.8		12.9	
5501-6000	5555	16							
	5613	15							
	5971	47	36.4	41	3.9	27.5	26	16.38	
6001-6500	6178	40							
6501-7000	6588	33	33						
	6798	41	15	30.5	13	16.75	13	11.7	
	6901	25							

Ductility Regression Analysis

Table 49: Test Results for Ductility-PG64-28

PG64-28

Analysis of Variance					
Source	DF	Sum of Squares	Mean Square	F Value	Pr > F
Model	1	16.29403	16.29403	0.21	0.6556
Error	15	1180.37422	78.69161		
Corrected Total	16	1196.66825			

Parameter Estimates						
Variable	Label	DF	Parameter Estimate	Standard Error	t Value	Pr > |t|
Intercept	Intercept	1	30.64988	3.72131	8.24	<.0001
elev1000		1	-0.45018	0.98931	-0.46	0.6556

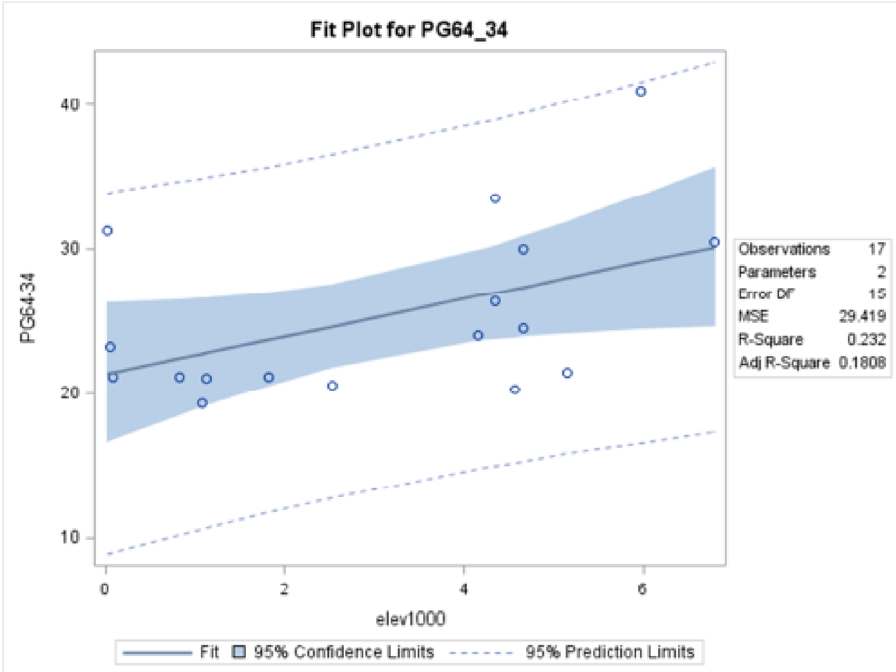

Figure 29: Ductility Fit Plot PG64-34

Table 50: Test Results for Ductility-PG64-34

PG64-34

Analysis of Variance					
Source	**DF**	**Sum of Squares**	**Mean Square**	**F Value**	**Pr > F**
Model	1	133.30080	133.30080	4.53	0.0503
Error	15	441.28950	29.41930		
Corrected Total	16	574.59029			

Parameter Estimates						
Variable	**Label**	**DF**	**Parameter Estimate**	**Standard Error**	**t Value**	**Pr > |t|**
Intercept	Intercept	**1**	21.37757	2.27535	9.40	<.0001
elev1000		**1**	1.28762	0.60490	2.13	0.0503

Table 51: Test Results for Ductility-PG70-22

PG70-22

Analysis of Variance					
Source	**DF**	**Sum of Squares**	**Mean Square**	**F Value**	**Pr > F**
Model	1	0.08395	0.08395	0.00	0.9504
Error	15	315.17944	21.01196		
Corrected Total	16	315.26339			

Parameter Estimates						
Variable	**Label**	**DF**	**Parameter Estimate**	**Standard Error**	**t Value**	**Pr > |t|**
Intercept	Intercept	**1**	10.62436	1.92294	5.53	<.0001
elev1000		**1**	0.03231	0.51121	0.06	0.9504

Table 52: Test Results for Ductility-PG70-28

PG70-28

Analysis of Variance					
Source	**DF**	**Sum of Squares**	**Mean Square**	**F Value**	**Pr > F**
Model	1	7.65643	7.65643	0.57	0.4605
Error	15	200.15416	13.34361		
Corrected Total	16	207.81059			

Parameter Estimates						
Variable	**Label**	**DF**	**Parameter Estimate**	**Standard Error**	**t Value**	**Pr > |t|**
Intercept	Intercept	**1**	17.27937	1.53239	11.28	<.0001
elev1000		**1**	0.30859	0.40739	0.76	0.4605

Table 53: Test Results for Ductility-PG76-22

PG76-22

Analysis of Variance					
Source	**DF**	**Sum of Squares**	**Mean Square**	**F Value**	**Pr > F**
Model	1	11.89946	11.89946	0.29	0.5963
Error	15	609.38290	40.62553		
Corrected Total	16	621.28235			

Parameter Estimates						
Variable	**Label**	**DF**	**Parameter Estimate**	**Standard Error**	**t Value**	**Pr > |t|**
Intercept	Intercept	**1**	22.32778	2.67381	8.35	<.0001
elev1000		**1**	-0.38471	0.71084	-0.54	0.5963

Table 54: Test Results for Ductility-PG76-28

PG76-28

Analysis of Variance					
Source	**DF**	**Sum of Squares**	**Mean Square**	**F Value**	**Pr > F**
Model	1	3.88262	3.88262	0.87	0.3649
Error	15	66.69688	4.44646		
Corrected Total	16	70.57949			

Parameter Estimates						
Variable	**Label**	**DF**	**Parameter Estimate**	**Standard Error**	**t Value**	**Pr > |t|**
Intercept	Intercept	**1**	13.01497	0.88458	14.71	<.0001
elev1000		**1**	0.21975	0.23517	0.93	0.3649